AD-A043 666 LOCKHEED MISSILES AND SPACE CO INC PALO ALTO CALIF PA--ETC F/G 4/1
IONOSPHERIC IRREGULARITIES: OPTICAL SUPPORT OF HAES SCINTILLATI--ETC(U)
JAN 77 R D SEARS DNA001-76-C-0182

UNCLASSIFIED DNA-4240F NL

1 OF 1
AD A043666

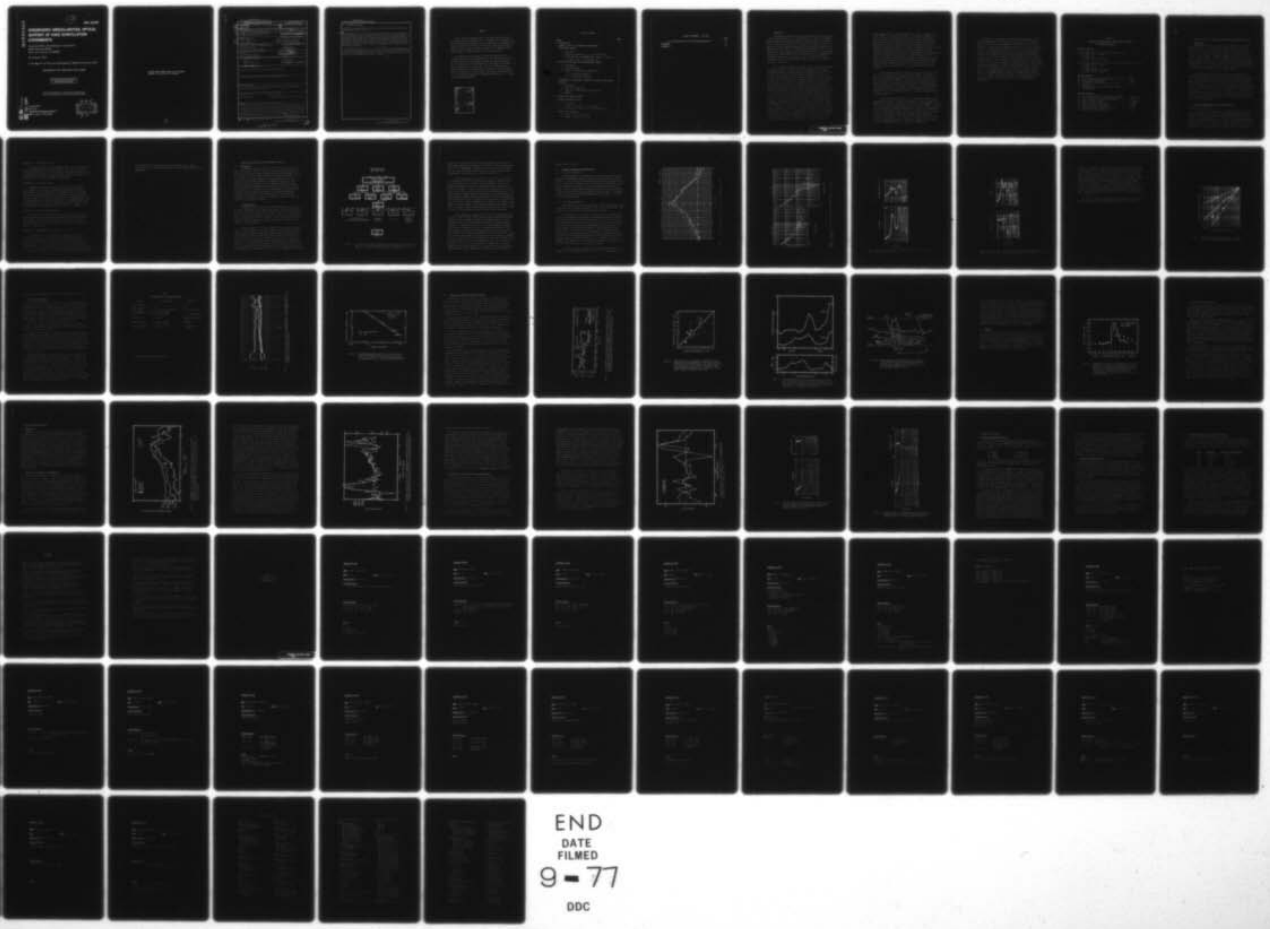

END
DATE FILMED
9-77
DDC

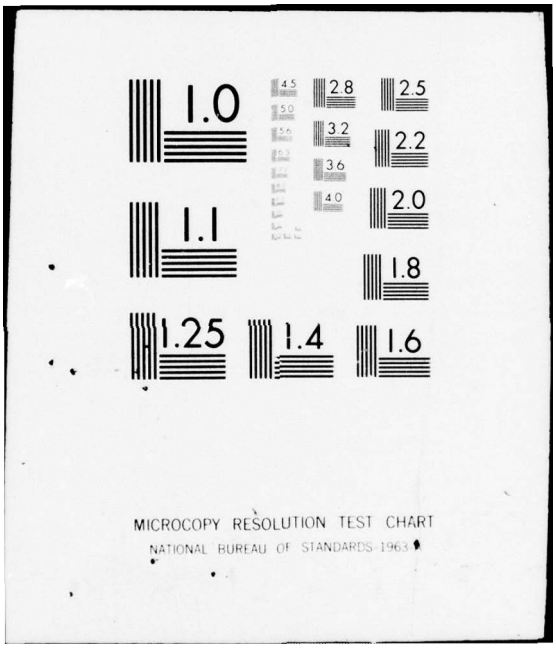
1.0
1.1
1.25
1.4
1.6
1.8
2.0
2.2
2.5
2.8
3.2
3.6
4.0
4.5
5.0
5.6
MICROCOPY RESOLUTION TEST CHART
NATIONAL BUREAU OF STANDARDS-1963-A

(12)

DNA 4240F

IONOSPHERIC IRREGULARITIES: OPTICAL SUPPORT OF HAES SCINTILLATION EXPERIMENTS

Lockheed Palo Alto Research Laboratory
3251 Hanover Street
Palo Alto, California 94304

31 January 1977

Final Report for Period 15 December 1975—31 January 1977

CONTRACT No. DNA 001-76-C-0182

APPROVED FOR PUBLIC RELEASE;
DISTRIBUTION UNLIMITED.

THIS WORK SPONSORED BY THE DEFENSE NUCLEAR AGENCY
UNDER RDT&E RMSS CODE B322076462 L25AAXHX63262 H2590D.

Prepared for
Director
DEFENSE NUCLEAR AGENCY
Washington, DC 20305

Destroy this report when it is no longer needed. Do not return to sender.

UNCLASSIFIED

SECURITY CLASSIFICATION OF THIS PAGE (When Data Entered)

REPORT DOCUMENTATION PAGE

READ INSTRUCTIONS BEFORE COMPLETING FORM

1. REPORT NUMBER: DNA 4240F
2. GOVT ACCESSION NO.:
3. RECIPIENT'S CATALOG NUMBER:

4. TITLE (and Subtitle): IONOSPHERIC IRREGULARITIES: OPTICAL SUPPORT OF HAES SCINTILLATION EXPERIMENTS.

5. TYPE OF REPORT & PERIOD COVERED: Final Report for Period 15 Dec 75 — 31 Jan 77

6. PERFORMING ORG. REPORT NUMBER:

7. AUTHOR(s): Robert D. Sears

8. CONTRACT OR GRANT NUMBER(s): DNA 001-76-C-0182

9. PERFORMING ORGANIZATION NAME AND ADDRESS:
Lockheed Palo Alto Research Laboratory
3251 Hanover Street
Palo Alto, California 94304

10. PROGRAM ELEMENT, PROJECT, TASK AREA & WORK UNIT NUMBERS:
NWED Subtask
L25AAXHX632-62

11. CONTROLLING OFFICE NAME AND ADDRESS:
Director
Defense Nuclear Agency
Washington, D.C. 20305

12. REPORT DATE: 31 January 1977

13. NUMBER OF PAGES: 90

14. MONITORING AGENCY NAME & ADDRESS (if different from Controlling Office): 85p.

15. SECURITY CLASS (of this report): UNCLASSIFIED

15a. DECLASSIFICATION DOWNGRADING SCHEDULE:

16. DISTRIBUTION STATEMENT (of this Report)

Approved for public release; distribution unlimited.

17. DISTRIBUTION STATEMENT (of the abstract entered in Block 20, if different from Report)

18. SUPPLEMENTARY NOTES

This work sponsored by the Defense Nuclear Agency under RDT&E RMSS Code B322076462 L25AAXHX63262 H2590D.

19. KEY WORDS (Continue on reverse side if necessary and identify by block number)

Auroral Intensity
Auroral Motions
Electric Fields
Precipitating Particle Energy Parameters

20. ABSTRACT (Continue on reverse side if necessary and identify by block number)

Photometric measurements of auroral spectral emission features and of the horizontal phase velocity of auroral motions were conducted at Chatanika, Alaska during several observing periods in 1976. These experiments provided ground-based optical support for the DNA HAES (High Altitude Effects Simulation) rocket experiments launched from Poker Flat. Data were obtained for the EXCEDE rocket flights of 28 February and 19 November as well as for the WIDEBAND coordinated rocket satellite experiment on 26 November 1976.

next page

DD FORM 1 JAN 73 1473 EDITION OF 1 NOV 65 IS OBSOLETE

UNCLASSIFIED

SECURITY CLASSIFICATION OF THIS PAGE (When Data Entered)

210118

20. ABSTRACT (Continued)

Additional experiments were conducted in coordination with the SRI/DNA incoherent scatter radar operation.

Multispectral data on the auroral emission intensities at 4278A and 6300A and the intensity ratio was analyzed in terms of the mean energy parameter for an assumed Maxwellian flux of precipitating electrons. Comparison between photometric determination of the mean energy parameter and that derived from incoherent scatter radar data provided a useful cross calibration of the two measurement techniques. This agreement also tends to confirm the theoretical predictions for the intensity ratio R_{64} I(6300)/I(4278) as a function of the mean energy parameter.

R sub 64

Additional analytical work was conducted to improve the three beam analysis code which allows inference of auroral E-fields and associated quantities from the auroral motion and intensity data. Results of the improved code are presented for the WIDEBAND rocket support experiment.

PREFACE

This is the final technical report on Contract DNA 001-76-C-0182 covering the period 15 December 1975 to 18 February 1977. The purpose of the research program reported herein was to determine the properties of the neutral and ionized consitituents in the auroral region by application of advanced optical sensing techniques in support of the DNA High Altitude Effects Simulation (HAES) experiments at Poker Flat, Alaska.

The experimental and analytical efforts were conducted at the Lockheed Palo Alto Research Laboratory and at the LMSC optical field site at Chatanika Alaska. The principal investigator on this program was Mr. R. D. Sears. Mr. D. E. Hillendahl also contributed to the program. We wish to acknowledge the support and assistance of Stanford Research Institute personnel at the Chatanika site, and the collaborative efforts of Drs. M. Baron and R. Vondrak of SRI. The support and encouragement of our colleagues at LMSC and of our DNA program officer, Dr. C. A. Blank are gratefully acknowledged.

TABLE OF CONTENTS

TABLE OF CONTENTS -- Continued

1. INTRODUCTION

The DNA/LMSC ionospheric irregularities program is a continuing effort to apply advanced optical remote sensing techniques to support the DNA/HAES (High Altitude Effects Simulation) program. These techniques and the instrumentation used were developed under the nuclear test readiness program and have been refined and improved during ground based experiments supporting the HAES program rocket launches at Poker Flat, Alaska during the period of 1972 through 1976. Optical ground based support has been provided to the ICE CAP program (1972-1976), EXCEDE (1975-1976), COMMOCAP (1974), and WIDEBAND (1976) experimental programs over this period. Results of ground based optical measurements made in years preceding the current contract are described in references 1 through 10.

The ionospheric irregularities program seeks to define certain spatial and temporal variations (irregularities) in the properties of the upper atmosphere by means of sensing the spatial and temporal structure in visible and near infrared spectral emission features generated in the region of interest. The atmospheric variables which are measured and those which may be inferred from the measurements are summarized in Table 1. These measurements and the related analyses are described in detail in the references. Two specific types of photometric instruments have been developed for this program:a multispectral (3 color) photometer which measures the spectral intensity of atmospheric emissions in three separate spectral regions through a single field of view; and a multibeam (3 beam) photometer which measures a single spectral emission intensity in three closely spaced fields of view. References 1 and 2 contain a complete description of this instrumentation. In general, the multispectral photometer is used to determine the temporal fluctuations of spectral emissions over a wide spatial region, for example, over a meridional scan, whereas the 3 beam photometers detect the short term temporal fluctuations and medium scale spatial variations (10's of km). The instrumentation is operated at the LMSC optical research site at Chatanika which is co-located with the DNA/SRI incoherent scatter radar. Two types of observations have been made. During periods of no auroras, the 3 color photometer may be used to verify the absence of auroral precipitation to

support EXCEDE and other rocket experiments which require a minimum level of auroral activity. Also during quiet times, the three beam measurements of emission intensity from the OH, Na, and O1 species may be used to infer neutral winds and detect wavelike motions in the relevant emitting regions. During periods of active auroras the three color photometer is used in a meridional scan mode to determine the latitude distribution of auroral electron and proton precipitation intensity, the total energy deposited in the atmosphere by these species, and the mean energy parameter of the precipitating electrons. The three beam photometers are generally operated in the O1 emission wavelengths of 5577A and 6300A in order to provide data on E region auroral motions (from which E-fields are derived) and the F-region irregularity structure which may be related both to inhomogenieties in the precipitation source and the generation of ionized irregularities by plasma processes.

The ionospheric irregularity program has been geared to provide data from which two basic types of information can be derived: the physical processes which create irregularities in both the ionized and neutral media which then exhibited as structure in visible and/or infrared emission; and quantities which can be measured in the visible and/or near infrared which can be directly scaled from the natural atmosphere to the nuclear disturbed atmosphere. In either case, the data base for constructing and verifying predictive codes for nuclear burst disruption to various systems is expanded by such measurements.

This report presents the results of the ground based optical support experiments during 1976. Photometric measurements were made in support of the EXCEDE rocket experiment in February and in support of the WIDEBAND coordinated satellite and rocket experiments during November. The ground based experiments and their specific relationship to HAES program objectives are summarized in section 2. Unfortunately because of weather and other problems, the ICE CAP series of rocket launches scheduled for February 1976 were postponed indefinitely. In addition to the specific rocket support observations made, a series of experiments related to expanding the capabilities of the multispectral and multibeam photometer observations was undertaken.

In addition to the experiments conducted at Chatanika during 1976 the analytical routines utilized to derive the wavelike properties of upper atmospheric motions and related quantities (see table 1) were improved significantly. These results are summarized in section 3. Section 4 contains a comparison of the SRI Untangle Code results with the optical determination of the mean energy parameter. We have shown, in collaboration with SRI, that both the total energy deposit and mean energy parameter derived by radar techniques and by optical techniques are self consistent and agree with theoretical predictions. These results have important implications with respect to utilization of optical techniques for determining effects of high altitude bursts upon the atmosphere, and the consequent systems effects, especially in the beta and debris deposition regions. Section 5 contains the results pertaining to the EXCEDE experiment and section 6 presents the preliminary results of our WIDEBAND support experiments. The summary and conclusions, section 7, contains an up-to-date assessment of the future utility of the ground based support optical experiments with respect to HAES program requirements.

TABLE 1

IONOSPHERIC IRREGULARITIES: PHOTOMETRICALLY MEASURED, AND INFERRED QUANTITIES

MEASURED QUANTITIES

A) Photometric intensities vs. time in same field of view
   1) 4278A N_2^+ E-region
   2) 4861A H^2 "
   3) 5577A O(1s) "
   4) 6300A 9(1D) E & F region

B) Photometric Intensities vs. time in three closely spaced fields of view
   1) 4278A N_2^+ E-region
   2) 5577A O^2(1S) "
   3) 5890A Na "
   4) 6300A O(1D) E & F region
   5) 7700-8100A, OH D-region

DERIVED QUANTITIES

C)	Energy Deposit by precipitating particles (total),	from A1
D)	Flux of precipitating protons,	" A2
E)	Photometric intensity Ratios,	" A4,A1
F)	Auto and cross spectra and related statistical quantities,	" B
G)	Horizontal phase velocity of motions of emission irregularities,	" F

INFERRED QUANTITIES

H)	Mean energy parameter of precipitating electrons,	" E
I)	Oxygen excitation and quenching chemistry kinetics,	" A3,A4,E,F
J)	Spatial structure of optical irregularities,	" F
K)	Auroral electric fields,	" G,(B1,B2)
L)	Pederson and Hall conductivities,	" C,D,E
M)	Joule heating in auroral regions,	" C,E,K
N)	Neutral winds and wavelike motions,	" F,G
O)	Frequency spectra of auroral E fields,	" G
P)	Large scale F-region structure,	" A4

2. SUMMARY OF THE 1976 IONOSPHERIC IRREGULARITIES EXPERIMENTAL PROGRAM

2.1 Introduction

Experimental operations of the photometric apparatus were conducted during two periods in 1976. During the February 10 to March 1 interval, observations were divided into two groups; those intended as exploratory measurements to extent the utility of the photometric techniques, and those oriented to direct support of EXCEDE and ICECAP rocket launches. The second period of operation, from 13 to 28 November supplied direct optical support to the WIDEBAND coordinated satellite and rocket experiments. The individual experiments which were conducted and their relationship to HAES program goals is summarized in the following sections. Table 2 digests the number of hours of data obtained with respect to each individual experiment.

It should be pointed out that the operational philosophy on the Ionospheric Irregularities program has been to obtain as much data relating to the specific experimental and analytical goals as is reasonably possible. Hence, photometric observations are normally made regardless of the rocket launch conditions as long as observing conditions permit. The experimental schedule is adjusted depending upon the rocket experiments which are counting down, and is also coordinated insofar as is practicable with the operation of the Chatanika incoherent scatter radar. The results of all of the following experiments are not discussed herein because limited financial sources did not allow adequate sampling and analysis of the large volume of data obtained, over 150 hours in 1976 alone.

2.2 Exploratory Experiments: 12 to 19 February 1976.

Experiment 1: E-field scans

This experiment was undertaken to determine whether auroral motions could be monitored at large off zenith angles such that E-fields could be inferred over a range of latitudes. We operated the 3-B-1 photometer at 5577Å on the scan head which was set to operate on 30 degree angle increments at zenith, 30° N and 60° N zenith angles in the magnetic meridian. Photometer 3-B-2 was operated also on 5577A but at zenith. One additional goal of the experiment was to determine whether 30 second data periods could be used to

TABLE 2

IONOSPHERIC IRREGULARITIES: HAES – 1976

Operational Summary

	Winter Period																			Fall Period					
Date/Tape No Experiment	2/10 1	11 2	12 3	13 4	14 5	15 6	16 7	17 8	18 9	19 10	20 11	21 12	22 13	25 14	26 15	27 16	28 17	29 18	3/1 19	3/7 20‡	11/14 1	11/15 2	11/19 3	11/22 4	11/24 5	11/2 6
1 E-Field-Scan 2 E Field Zenith		7	7	7	8		2	4	1.5	8																
3 AIW/AGW	5												4		3	2.5	8	7	4	6						
4 D&E Winds							5	2.5	6			.5	2	4.5	3	3										
5 E&F Winds						4					8	7.5		1					2.5							
6 EXCEDE																	*						*			
7 SWIR/SWIR/TMA																										
8 WIDEBAND (See No. 5 for description)																					1		3	6		4
Coordinated Rocket and Satellite Passes (known)									RICE Rocket 0706 UT								EXCEDE + UTD Rockets 0547 & 1212 UT		RICE Rocket 1046 UT		H_2O Rocket 0318 UT	Systems Checks	Excede Rocket 0406 UT		Systems Checks	Wideband Rocket 1025 UT
ISIS					+	+			+																	
TRIAD				+	+	+	+	+		+	+	+														
AE-C				+	+		+																			
S3-2					+	+	+																			
Operating Hours (on data)	0705-1255	0550-1300	0520-1720	0520-1300	0440-1305	0645-1100	0535-1310	0500-1250	0500-1300	0510-1350	0525-1310	0450-1250	0500-1150	0430-1220	0520-1200	0500-1100	0500-1250	0500-1230	0505-1145	0600-1215	0215-0900	Cloudy	0325-1105	0335-1030	Cloudy	0740-1120

*Data obtained in Exceed Support Mode.
‡Operations continued until 3/12 but no useful data were obtained because of cloudy weather.

infer E-fields instead of the 300 second periods previously used for this part of the experiment, the 3-B-1 scan dwell time was set at 30 seconds for each angle. Thirty second intervals taken at zenith will allow comparison directly between 3B1 and 3B2 results. We conducted this experiment in hopes of obtaining corroborative data from satellites S3-2 and Triad.

Experiment 2: E-field at zenith.

The data from 3B2 in experiment No. 1 will be used to infer E-field structure and temporal variations for comparison with Chatanika radar and satellite results.

2.3 EXCEDE, ICECAP, and WIDEBAND Rocket Support 20 February to 7 March 1, and 13 to 28 November 1976.

Photometer Configuration: Wavelengths as Before:

3 Color: Scan head
3-B-1: Zenith
3-B-2: Zenith

Experiment 3: AIW/AGW* studies

Here, we hoped to measure wave-like events in the auroral precipitation as observed by photometer 3B2 and in the Na layer as observed at 5890A on photometer 3B1. Previous data indicates that a dispersive type of auroral motion spectrum is observed both in the auroral E-region and in the Na layer when AIW's are generated. We will coordinate these measurements with Wilson's ground based detection of auroral AIW's. Energy deposit by precipitating particles in the auroral E-region is monitored with the 3C scanning photometer and by the photometer 3B2 for Joule heating input. Large enhancements in total energy input such as on 10 March 1975 may create large AGW's which may manifest themselves as TID's† at large distances from the auroral region. These wavelike motions may excite IR-active species at large distances from the auroral region.

*AIW: auroral infrasonic wave
AGW: acoustic gravity wave
†TID: travelling ionospheric disturbance

Experiment 4: D and E-region winds

During quiet periods, the three beam photometers will be operated on Na and OH wavelengths such that the winds and/or wave-like motions in the OH (85 km) and Na (95 km) regions can be monitored. These data will add to those obtained in 1975. Transport of excited IR-active species is important to the understanding of the spatial structure of IR emission.

Experiment 5: E and F-region winds

Simultaneous operation of the 3 beam photometers on the 5577Å and 6300 A emissions of O1 will allow inference of the winds and wave-like irregularities in the E and F-region in quiet periods, and of the E-region auroral motions and their effects upon the F-region irregularity structure and winds during active periods. We hope to be able to monitor F-region winds even during the presence of auroral disturbances. For WIDEBAND support, the 3 color photometer is operated in a meridional scan mode to provide precipitating particle total and characteristic energy values vs. latitude.

Experiment 6: Excede Background definition

The 3C photometer was operated in a scan mode in order to monitor background auroral emission during the EXCEDE shot. Photometers 3B1 and 3B2 were operated on 5890A and 5577A wavelengths respectively to detect the possible presence of wave-like disturbances in the neutral atmosphere in the Na and O1 emitting regions.

Experiment 7: SWIR/SWIR/TMA events (these shots not run)

The 3C photometer will be operated in a meridional scan mode to determine energy input to ionosphere from precipitating particles and to estimate the mean energy of the electrons. A time history is required. 3B1 will be operated on 5890A to obtain the winds in the 95 km region before, during, and after the events. Comparisons of the photometric data with the TMA trail will allow calibration of this photometric wind measurement technique. 3B2 will be run on 5577A wavelength in order to measure the energy deposit by

Joule heating in the vicinity of the rocket trajectory up leg. Auroral E-fields will also be inferred from these data. This experiment was postposed indefinitely.

3. THREE BEAM DATA ANALYSIS CODE IMPROVEMENTS (NUWAV10)

3.1 Introduction

The computer code used to process the three beam data such that the spatial and temporal variations in airglow and auroral emission may be interpreted in terms of neutral winds, auroral motions, wavelike phenomena, etc. has a variety of internal functions which are assigned to subroutines plus the control program. It became apparent that certain subroutine functions, especially the input/output routines were inadequate to handle the range of parameters required to describe the several different physical phenomena causing the measured fluctuations, hence improvements in the code to handle these parameters were instituted. The code improvements are described functionally in the next section and examples of the enhanced input/output capabilities are presented in the following section. A more detailed description of the function of the basic analytical code plus its important algorithms is contained in reference 3.

3.2 Code Improvements

The functional organization of the three beam analysis code involves statistical processing of three simultaneous digital time series as input data. These data are read off library copies of the field data records by the main program and the pertinent channels are placed in a data array. The processing steps are functionally described in figure 1. Here, the important statistical quantities which are computed are blocked out and the flow through the wave analysis section is displayed.

A major modification to the data input and control routing was made in order to compress successive five minute samples of data within the 300 unit sample length of the basic computation. Because successive intensity samples are recorded nominally every second, with a 300 second series making up one digital record, it was necessary to perform boxcar averaging on successive n units of data in each time series in order to obtain an overall compression factor of n. We have tested this aspect of the code up to a value of n = 12, i.e., a one hour interval of data compressed into the 300 sample time series. The consequencies of such compression of the data is a shifting of the frequency

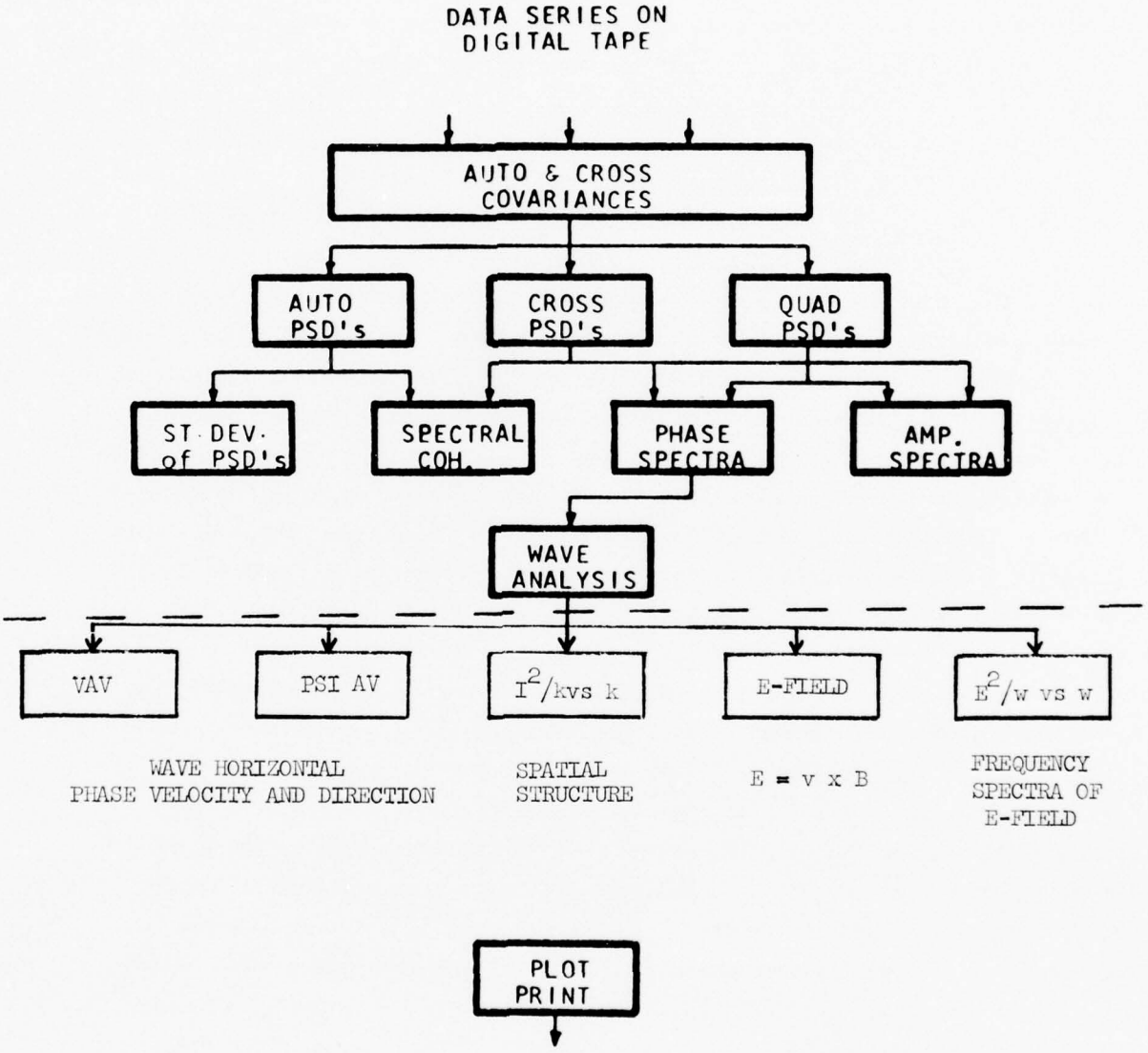

Figure 1 Flow diagram of computer program used to analyze three beam photometer data. The improved subroutines for obtaining average phase velocity, direction, etc. are those indicated below the dashed line.

window for the statistical and wave analysis parameters by a factor of 12. This frequency window shift hopefully will allow us to explore the dispersive effects of the Brunt-Vysala frequency and acoustic cut off region (around 0.003 Hz, 5 min period) upon wavelike phenomena in both the neutral atmospheric emission and in the motion of auroral excited species.

As the code previously existed, each of the statistical quantities was independently provided as both tabular and graphical output but little post processing on the wave analysis data was performed. The important functional modifications to the wave analysis code are described below the dashed line in figure 1. Here, the wave analysis output in terms of the wave phase velocity spectra are post processed to provide weighted averages of the three redundantly computed phase velocity spectra. The weighting function is derived from the coherence spectra such that pairs of time series exhibiting high coherence levels play a stronger role in the computation of average phase velocities than the channels exhibiting lower coherence. In addition to these outputs, the spatial spectra of the emission fluctuations are computed. This involves a simple coordinate transformation between the power spectral density data and the horizontal phase velocity at a given spectral frequency.

Because much of the interpretation of the three beam photometer data has been in terms of auroral motions and the E fields which may be inferred therefrom, we have included both tabular and graphical output of several quantities related to E fields, namely the equivalent E field geometrical components (vs. frequency) and a plot of the E field fluctuation spectrum separated into north-south, and east-west geomagnetic coordinates. Both of these outputs are useful when comparing auroral motion data and inferred E fields with other experimental measurements of the same quantities. Finally, the plot/print output routine was altered to conserve resources by combining plots of the same or closely related parameters on the same coordinate system. Although the major goal of the code improvement effort was to enhance the useability of the code, a minor improvement in running time was realized (approximately 20 seconds CPU time for each three channel record segment of 5 minutes duration) and the output volume in both plot and print formats was

reduced a factor of three.

3.3 Examples of Improved Code Applications

3.3.1 Statistical Parameters

The major changes in the subroutines for plotting out the statistical parameters is reformatting them such that more than one parameter is provided per plot. The new formats for correlation function, and power spectral density plots are illustrated in figures 2 and 3, for periods of active auroras. The abcissa coordinates of the plots are now self adjusting such that when the spectral window is changed by the reformatting of data in the control program, the data are presented in the proper frequency coordinate window. Reformatted plotting of the other statistical parameters specified in figure 1 is similar to those illustrated herein.

3.3.2 Wave Analysis Parameters

The weighted wave velocity and directional spectra which are new outputs of the program are illustrated in figure 4. Here, one can readily detect wave dispersive velocity effects in both magnitude and direction.

For applications of the analyses to auroral motions and determination of the auroral E-fields, the equivalent E-field frequency spectra are printed out rather than plotted. The reason for this choice is that the selection of an equivalent E-field value is normally based upon either the lowest frequency point or the lowest velocity point, depending upon relative coherence levels and the shape of the phase velocity spectrum. The listing provides these values related to the geomagnetic coordinate system as E (north-south) and E (east-west). Fluctuations in equivalent E-field vs. frequency are directly relateable to other experimental measurements, however, and these spectra are plotted, again vs. geomagnetic coordinates, i.e., $E^2(N\text{-}S)/\omega$ vs. ω and $E^2(E\text{-}w)/\omega$ vs. ω. Sample cases of these spectra are presented in figure 5 a and b, for the same data interval as the previous examples.

The final wave analysis output which is plotted is the spatial frequency plot of the intensity fluctuations, I^2/k vs k. A typical plot of this

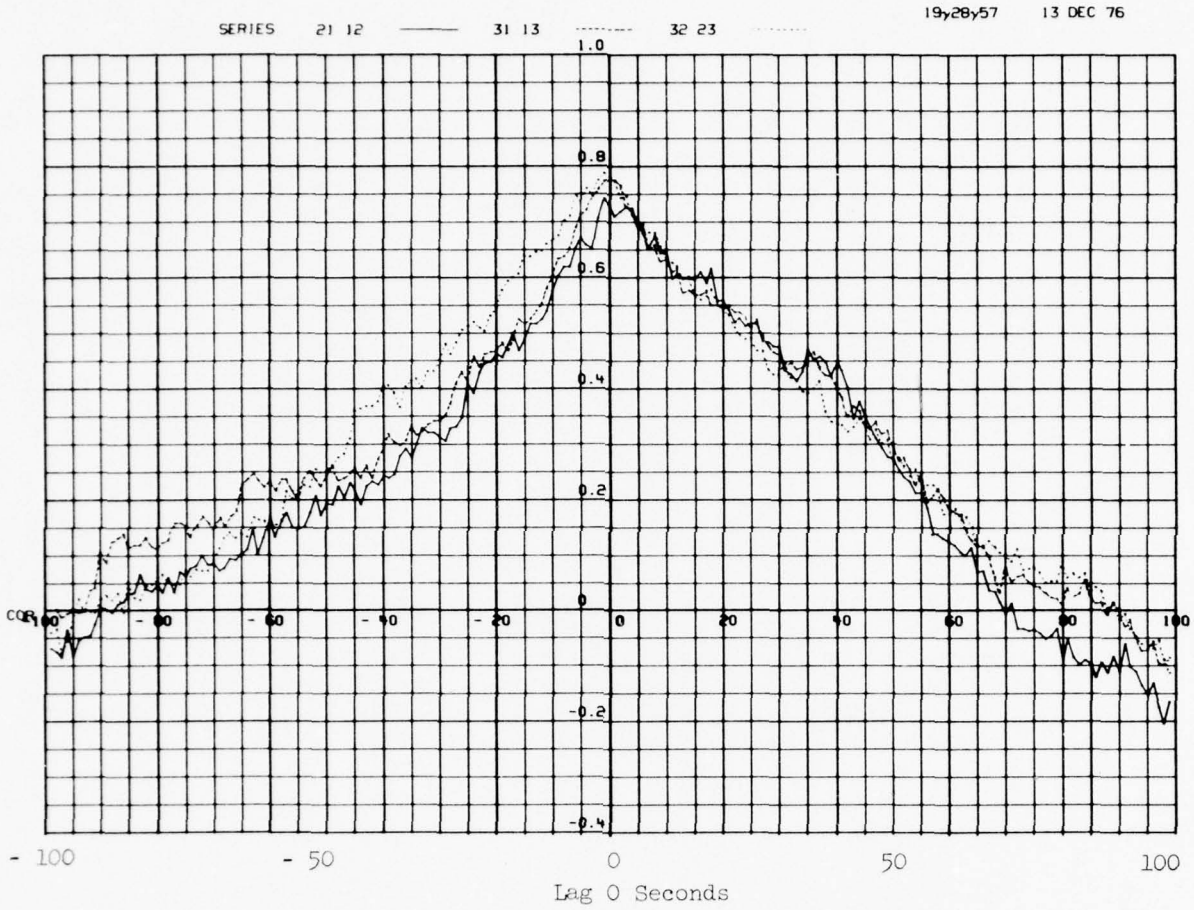

Figure 2 Plot of cross correlation vs. lag index for 3 beam photometer data.

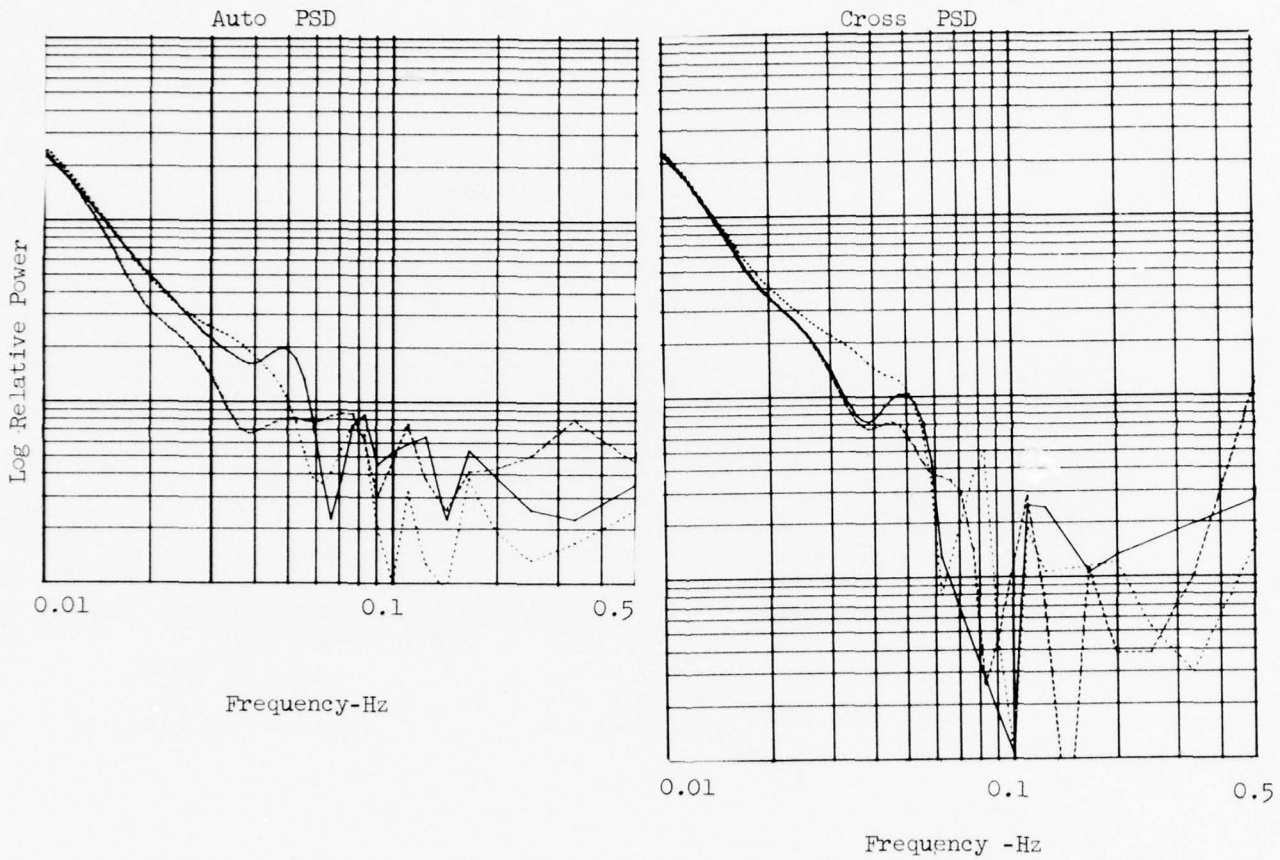

Figure 3 Auto and cross power spectral densities (PSD) revised plot format. Same data as figure 2.

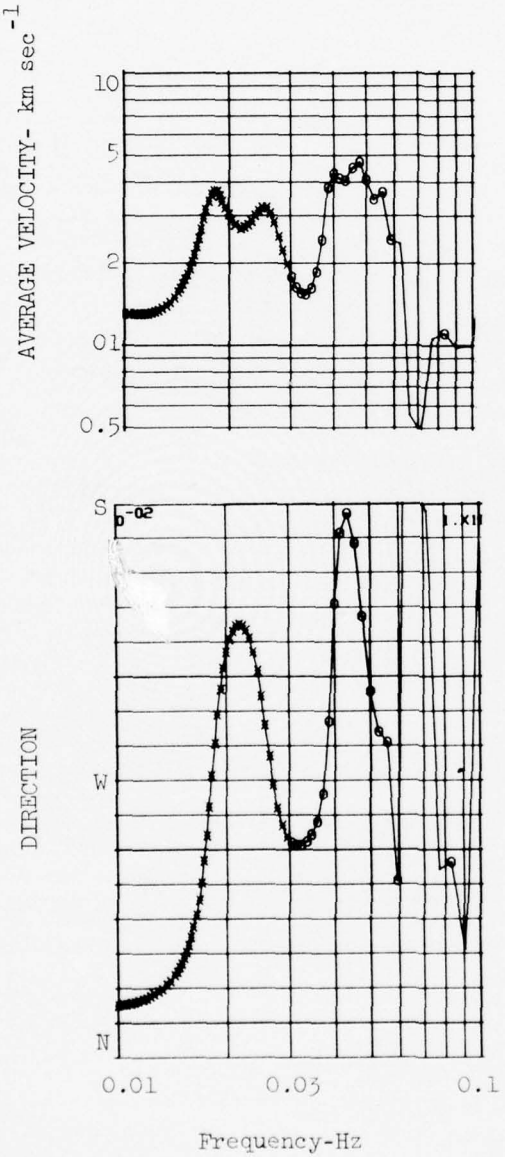

Fig. 4 Wave velocity and direction computed by weighted averaging of three sets of wave phase velocity vectors.

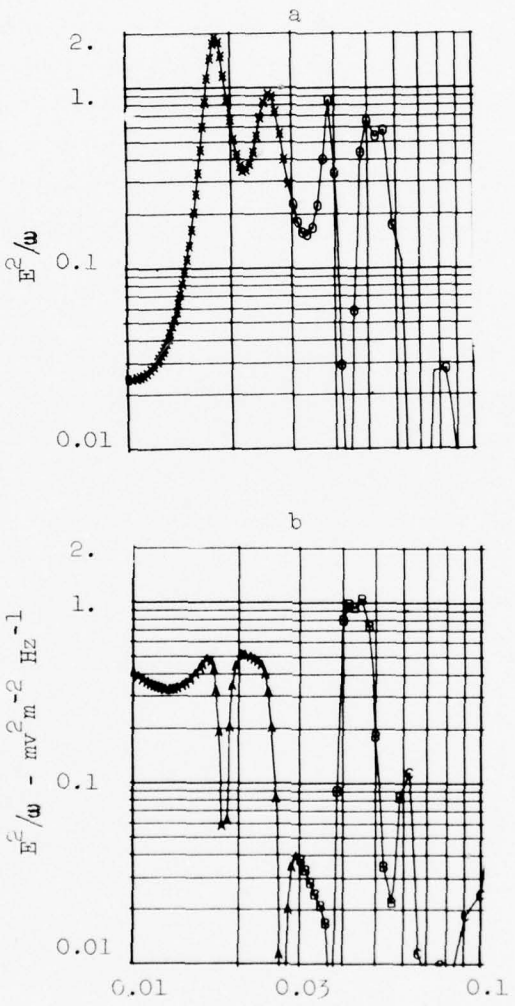

Figure 5 Electric field fluctuation spectra inferred from auroral velocity spectra of fig. 4. Curve A is N-S component; curve b is E-W component.

spectrum is illustrated in figure 6. Here, one notices the irregular behavior of this spectrum, and more surprisingly, the positive average slope vs. the expected negative slope. We have not run enough auroral motion data samples since the code improvement to determine whether this is an artifact of the coordinate change routine in the code or whether it is a real physical effect. The irregular nature of the spectrum can be removed by smoothing and by invoking weighting functions as was carried out in the computation of the average velocity parameters. Resources available to the program did not allow resolution of these problems, but they were not degradatory to the interpretation of the optical ground based support data for the various HAES experiments conducted this year.

The results of applying the improved wave analysis code to the various HAES experiments during 1976 are discussed in detail in later sections.

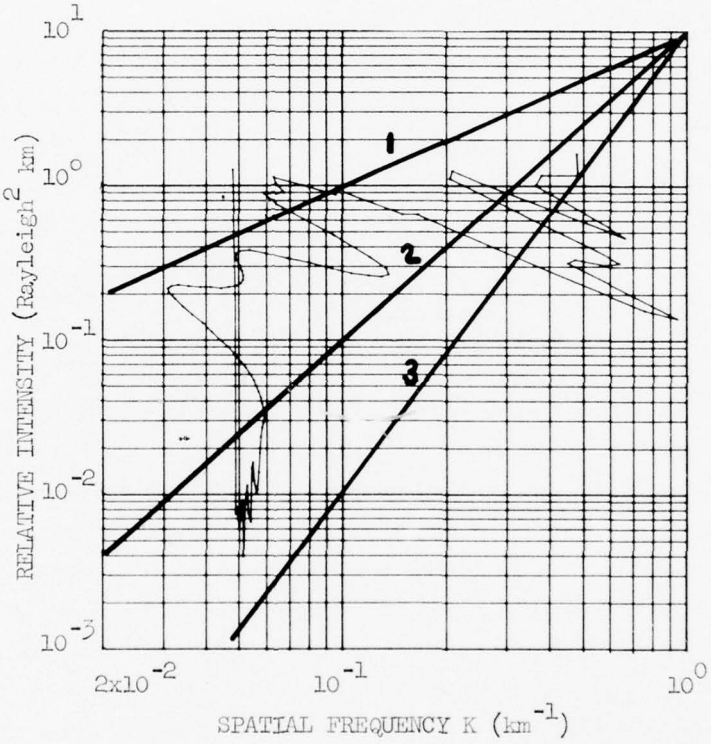

Figure 6 Spatial frequency spectra of auroral emission. Heavy lines denote k^n spectrum where n = 1,2,&3.

4. DETERMINATION OF MEAN ENERGY PARAMETER FOR AURORAL PRECIPITATING ELECTRONS

4.1 Introduction

Systematic emission altitude variations in the relative intensities of auroral ionization source strength and of spectral emission features have been known since the early spectroscopic measurements of Vegard (see reference 11 for a discussion of the early work). These intensity variations are related to the mean energy of the precipitating particles because particles of different mean energy deposit the main portion of their energy at different altitudes depending upon the atmospheric density. Only in the past few years has it been possible to predict with confidence the altitude dependence of many important auroral spectroscopic emission features because of the complexity of the interactions between the particles of different energy distribution and pitch angle distribution with the atmosphere.

Theoretical models of the altitude dependence of N_2^+ 1st negative band emissions at 3914, 4278, etc. and of O1 forbidden emission features at 5577 and 6300A have been published by Kamiyama (12), Banks et al (13), Judge (14), and by Rees and Luckey (15). Of particular value to the interpretation of ground and aircraft based photometric observations is the predicted variation of the ratio $R_{64} = I(6300)/I(4278)$ as a function of the mean energy parameter for precipitating auroral electrons. The mean energy parameter α is one half the average energy if the energy distribution of the precipitating particles is assumed to be Maxwellian, i.e., $F(E) = F_o E \exp(-E/\alpha)$. The assumptions and physical limitations of such multi-parameter models are discussed in detail in the references cited above. Their main limitations however, appear to be related to the errors caused by variations in atmospheric density vs. altitude from the model used, and by departure of the precipitating electron energy flux from a Maxwellian spectrum. Despite these potential sources of error, we show that the ration R_{64} is a useful measure of the mean energy parameter.

Empirical relationship of the total energy deposit on the atmosphere by precipitating particles to spectroscopic emission intensities has been carried out by a number of investigators. For example, Wickwar et al (16) demonstrated that energy deposit derived from photometric measurements of the auroral

4278A N_2^+ band intensity compared well with that derived from incoherent scatter radar measurement of the height profile of ionization. Because, the altitude variations of recombination coefficients in the auroral E-region as well as the fluorescence efficiency for production of the 4278A emission by incident particles now are both reasonably well known, these measurements not only provided a useful cross calibration of the radar and photometric measurement techniques, they also confirmed theoretical predictions. Additionally, comparisons (17) of rocket and satellite measurements of the incident electron flux total energy with photometric data also confirm the N_2^+ 1st negative band fluorescence efficiency values obtained in the laboratory.

Various attempts to confirm the theoretically predicted R(6300/4278) value have been made, but to date none have provided definitive confirmation of Judge's (14) or Rees and Luckey's (15) predictions over a wide range of auroral conditions. Mende and Eather (18) compared airborne photometric measurement on a rather weak aurora (100 R of 4278A emission) with satellite particle data obtained on OV1 18. Their single comparison was consistent with the Rees and Luckey prediction but cannot be considered definitive because the photometer field of view and the subsatellite geomagnetic field region did not physically intersect. Other comparisons have been made using rocket borne electron detectors, and on-board and ground based photometers, but the problems of non coincident experimental volumes and temporal and spatial fluctuations in auroral characteristics have precluded definitive confirmation of the ratio values, except perhaps for few special cases.

In this report section we describe the derivation of the mean energy parameter from optical observations of the R_{64} ratio value for two cases, observations at magnetic zenith, and observations in a meridional scan mode. These observations are then compared with coordinated observations made with the Chatanika incoherent scatter radar. The radar observations of electron density vs. altitude were analyzed in terms of the energy flux of the precipitating electrons by means of the SRI UNTANGLE code (19). The mean energy parameter for the precipitating electron flux is then compared with that obtained optically. This comparison provides an empirical cross calibration between the two measurement techniques, but more important, because the two techniques differ completely in their analytical basis, their quantitative

agreement tends to substantiate the theoretical predictions of R_{64} vs. α.

4.2 Photometer Measurements

The three color photometer was operated in close coordination with the Chatanika incoherent scatter radar on several occasions during 1975 and 1976. Comparative measurements of the mean energy parameter are presented herein for two periods; 12 March 1975 during the Multi-rocket launch window, and 20 February 1976. During the 1975 Multi-support experiment the photometer and radar were both operated in meridional scan modes, but with asynchronous timing. During 20 February 1976 both the radar and photometer were operated with superimposed fields of view pointed at geomagnetic zenith.

Details of the operation of the photometer, calibration procedures, etc. have been described in previous publications. Pertinent photometer characteristics are summarized in Table 3.

An example of the calibrated data output for the 20 February operational period is illustrated in figure 7. Here, the temporal variations in auroral intensity in the 4278A and 6300A spectral emissions and the contemporaneous ratio variations are plotted for a single five minute observing period (1 data record) on a second by second basis. The auroral intensity during this period exhibited only slow variations and the ratio variation was even smaller, indicating a nearly constant electron energy deposit and mean energy parameter vs. time for this period.

The mean energy parameter is derived from the R_{64} value by applying the Rees-Luckey relationship which is summarized graphically in figure 8. The curve simplified the theory in that the slight dependence of R_{64} upon total energy deposit (i.e., I(4278)) is not included in this curve, but the range of values for $0.1 \leq \alpha \leq 10$ kev is indicated by the bars. Because the normal auroral mean energy parameter ranges between about 1 and 10 kev., ignoring the total energy dependence causes an error in the estimated value of α from empirical values of R_{64} of only a few percent. In the next section, we compare the values of mean energy parameter obtained from the photometer technique with contemporaneous values obtained from application of the UNTANGLE code to the incoherent scatter radar observations.

TABLE 3

PHOTOMETER AND RADAR CHARACTERISTICS

Parameter	Photometer Value	Radar Value
Field of view	3°	0.4°
Range resolution	none	6 km
Sensitivity*	> 1.0 Rayleighs (at 4278A)	> 10^{4} electrons/cm^{3}
Sensitivity* to ionization source in column	> 0.005 erg/cm^{2} sec	> 2 x 10^{-3} erg/cm^{2} sec
Scan rates	2 deg/sec.	variable but usually slower
Scan increments	10 degrees (1975) 4 degrees (1976)	continuous
Integration times	1 second or longer	1-2 seconds and longer

* Estimates based upon best conditions

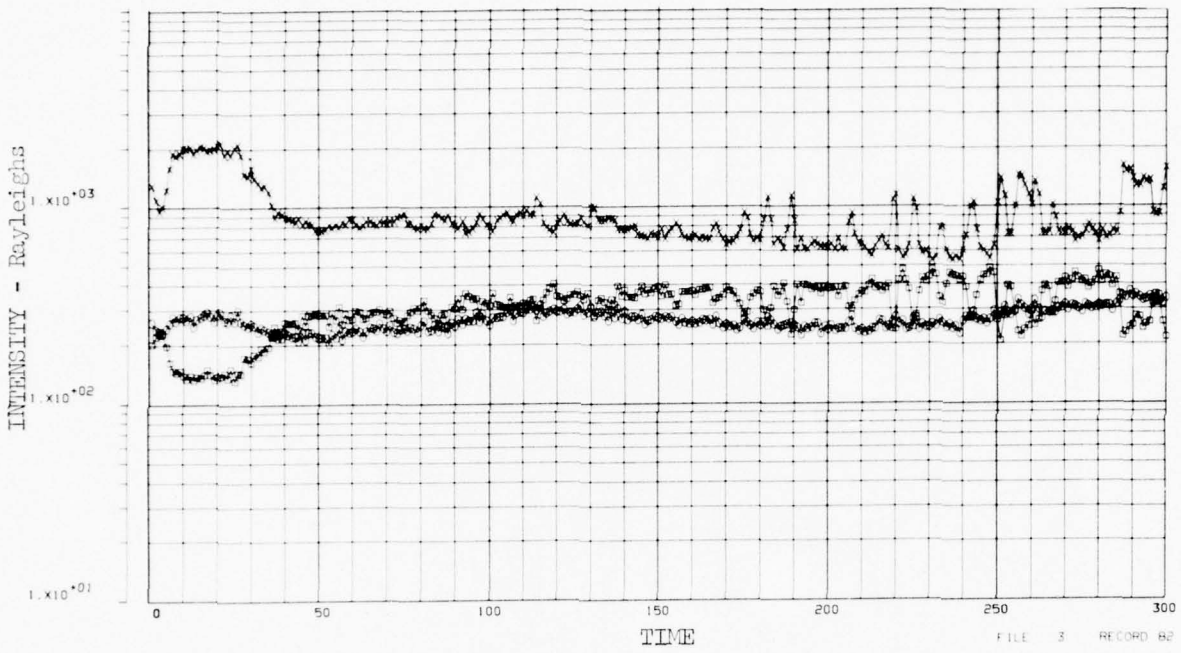

Figure 7 Calibrated values of 4278 Å and 6300 Å intensities for 5 minute record period on 20 February 1976 and their ratios. X-indicates 4278 Å, O-6300 Å, □-R64 ratio x 1000. Beginning time of record is 1155 UT.

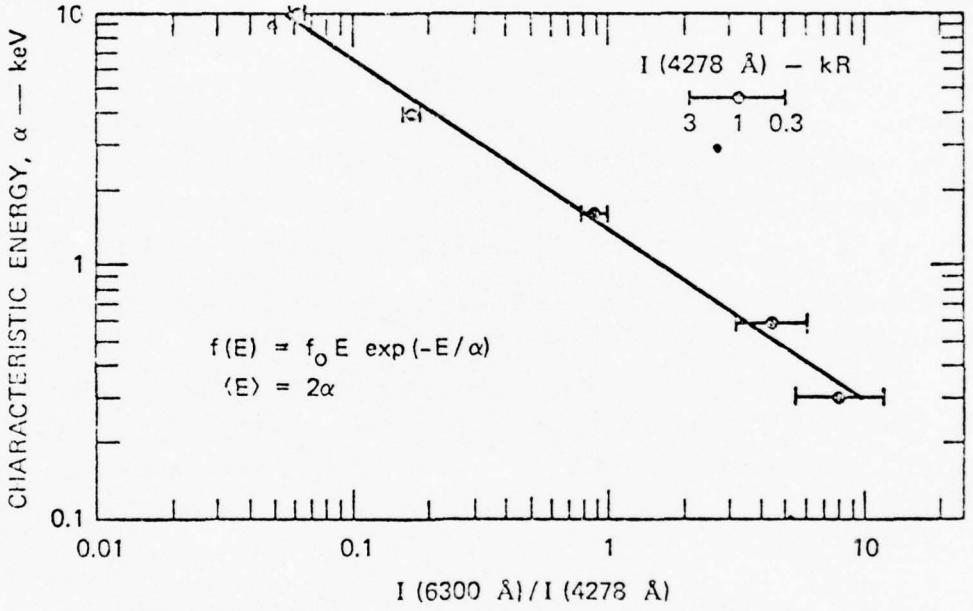

Figure 8 Characteristic energy parameter vs. intensity ratio R_{64} = I(6300/I(4278) derived from Rees and Luckey theory in reference 15. The horizontal bars indicate the dependence of R_{64} on auroral intensity I(4278 Å).

4.3 Comparison of Photometer and Radar Results

Coordinated observations were made on the night of 20 February 1976 with both the incoherent scatter radar and the photometer pointed at geomagnetic zenith. In order to understand the detailed comparisons of the mean energy parameter data, the pertinent characteristics of the photometer and radar are listed in Table 3. Active auroral conditions persisted during the entire observing period, 1040 to 1200 UT. After a substorm occurred at about 1110 UT, amorphous aurora covered the entire sky.

Figure 9 illustrates segments of the comparative measurements analyzed in terms of mean energy parameter. Both data sets were reduced with integration time of 20 seconds. Both data sets produced closely comparable results for the mean energy parameter except for a few unique periods when radar derived mean energies are much harder than those determined photometrically.

This effect is undoubtedly caused by the patchiness of the aurora such that the radar briefly observed a small scale hardening which was integrated out over the photometer field of view. These data as well as other comparable data obtained on 20 February are presented as a correlation plot in figure 10. Here, although some scatter is observed, most of the points agree within about 20 percent, which is within the mutual experimental errors of the two experimental techniques.

Scanning experiments were conducted during the 12 March 1975 Multi-rocket experimental period. During part of this period of coordinated observations, a bright arc was observed near zenith. Repeated scans through this arc region were made by both the radar and photometer, however, with asynchronous timing. Figure 11 illustrates the photometer scans through this region, showing the intensities of 4278A, 6300A, and R_{64} intensity ratio vs. zenith angle. A comparable view of the arc is provided by the incoherent scatter data (provided by R. Vondrak, of SRI) in figure 12. The radar scans show the narrowness of the arc but do not provide as high temporal resolution of the arc's motions as the photometer scans. Unfortunately, during 1975 the meridional scan mode was operated with a 10 degree angle increment step, thus the spatial resolution across the arc is much poorer than that provided by the radar. Despite the discrepancies in measurement parameters and operational modes, we were able to obtain a number of period of comparable data,

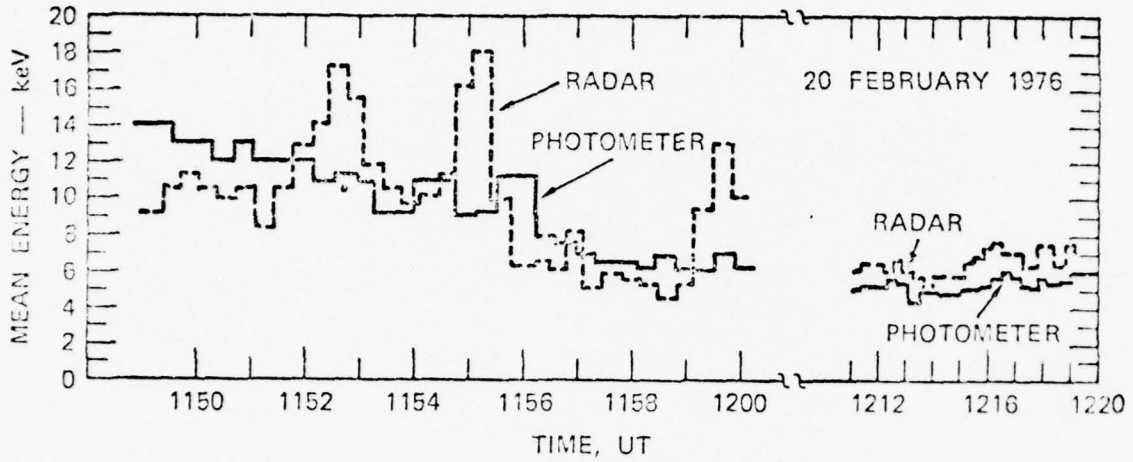

Figure 9 Time variation of mean energies for precipitating particles computed from photometric and radar data, 20 February 1976. Agreement between these independent techniques is good except for short periods when radar observes small scale hardening events which are unresolved to photometer.

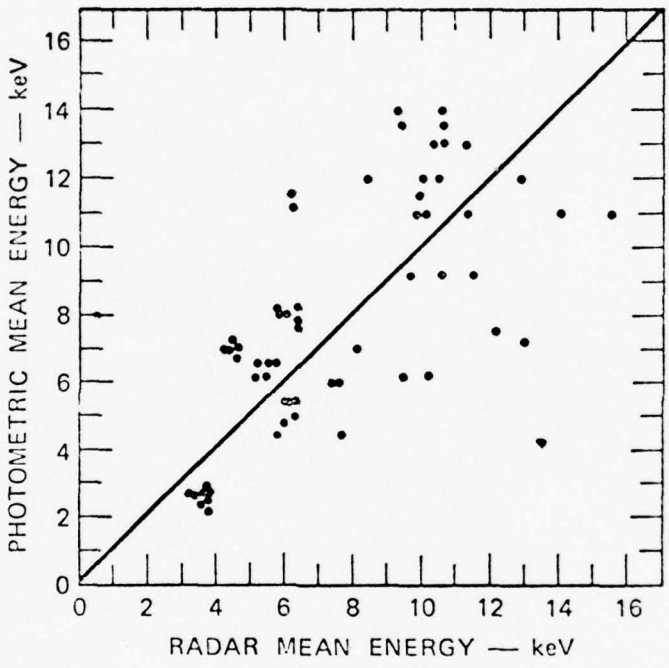

Figure 10 Correlation plot of comparative measurements of mean energy derived from photometric and incoherent scatter radar data for 20 February 1976. Each point represents a 30 second average. The cluster of points at low energy represents approximately 50 data points obtained during a period of constant energy input.

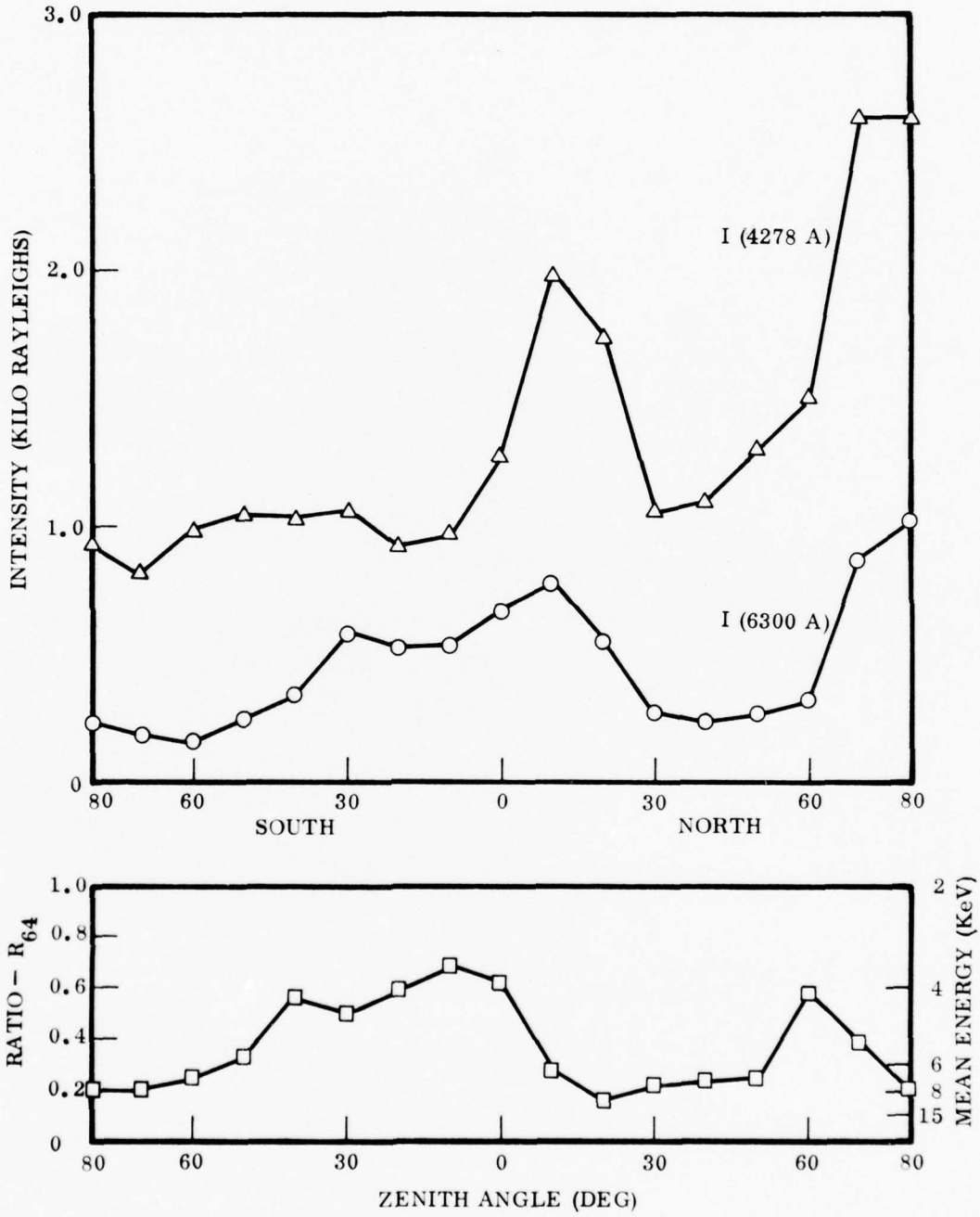

Figure 11 Calibrated photometer scans through arc region on 12 March 1975. Intensity of 4278 Å and of 6300 Å emission is plotted together with their intensity ratio, R_{64}. Note that for these data, the scan position increment was 10 degrees with a dwell time of 5 seconds at each position.

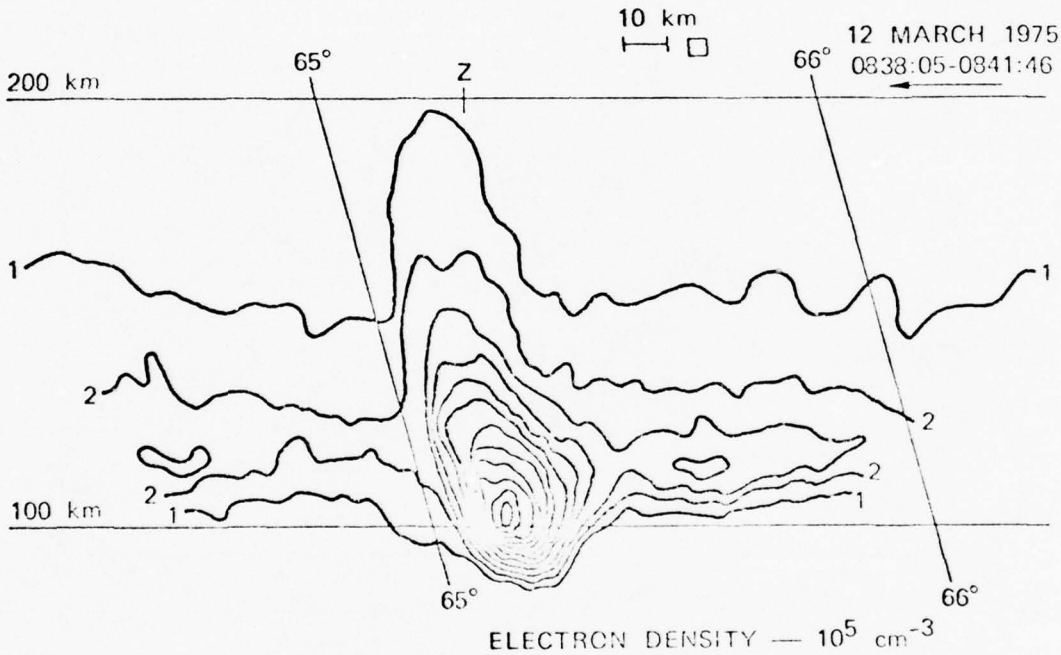

Figure 12 Contour map of electron density vs. height measured by the Chatanika incoherent scatter radar during a meridion scan. Contours are in units of $10^5/cm^3$ and are given in intervals of 1,2,4,5,6,8,10, etc. Data furnished courtesy of SRI.

i.e., when the photometer and radar were looking at the same portion of the sky at nearly identical times. Results of one such comparison are illustrated in figure 13. Here, the radar scan has been integrated over 10° angles to make its field comparable to the photometer. The fields of view generally coincided spatially within about 30 seconds. We see that the radar has outlined the energetic portion of the arc more adequately than the photometer, but both techniques produce closely comparable values of mean energy parameter in the diffuse precipitation region to the south of the arc. The moderate disagreement between the techniques at angles to the north of the arc are probably due to the differing geometry of the two measurements.

4.4 Summary

We have shown that the Rees and Luckey theory relating the mean energy parameter for precipitating electrons to the photometric R_{64} ratio agrees well with measurements of the mean energy independently derived from incoherent scatter radar measurements as analyzed by the UNTANGLE code. Such agreement provides cross calibration between the experimental techniques and furthurmore tends to confirm the predictions. Applications of these results to the WIDEBAND rocket launch is described in a later section.

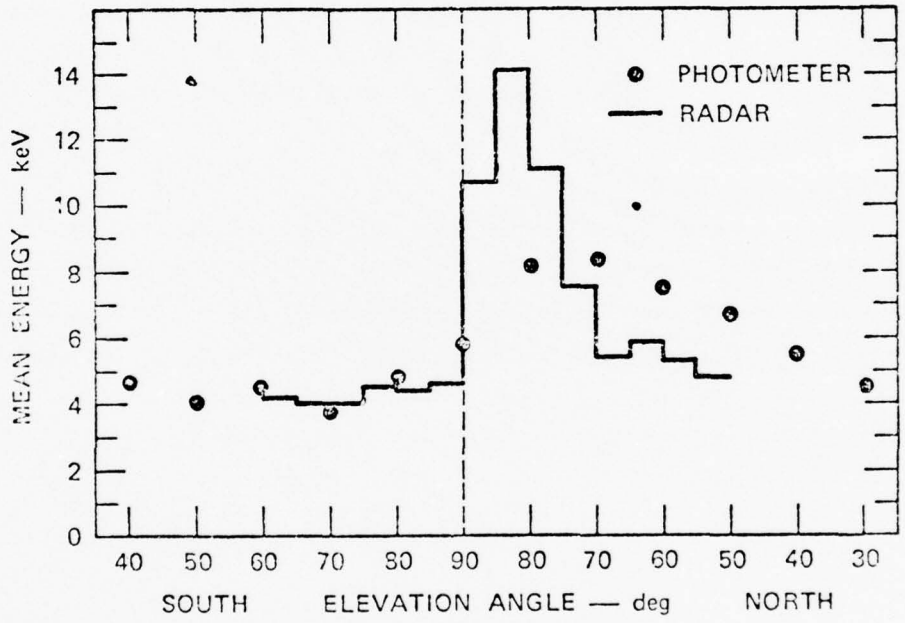

Figure 13 Comparison of mean energy for precipitating electron flux derived from radar and photometric measurements during scan operations in meridional plane. Data for 12 March 1975. Radar data are integrated over 10° scan angle to correspond with photometer angle increment setting. Narrow arc near zenith was missed by the photometer.

5. EXCEDE ROCKET SUPPORT RESULTS

Excede rockets were fired on 28 February and 19 November 1976. Our support for these experiments was mainly limited to confirming that the launches occurred during low levels of auroral activity such that the electron gun excitation in the visible and infrared was not appreciably contaminated by ambient auroral ionization and emission processes.

Data was obtained in support of EXCEDE experiments by the three color photometer operated in a meridional scan mode. During the February operation scan angle increments were set to 10 degrees with a 5 second dwell time. During the November period, a scan angle increment of 4 degrees was chosen, with a 2 second dwell time. Both scan programs allowed a full scan between 10 degree elevation angles in 80 seconds, i.e. 2 degrees per second. We found that the advantage of the shorter integration time and smaller scan angle increment made up for the somewhat larger statistical error in calibrated intensities because smaller scale and/or shorter time features exhibited in aurora arcs could be defined better in the new scan program.

Figure 14 illustrates the photometric intensities vs. scan angle for the February EXCEDE event. It is clear that a low level of auroral activity existed on the upleg trajectory, although some activity is present to the north.

The November EXCEDE data are likewise presented in Figure 15. Again, the activity level is lower on the upleg trajectory. In both cases, it is apparent that the rocket shots were conducted early enough that the uplegs passed equatorward of the main part of the diffuse precipitation flux is low as well as the energy parameter, i.e. the maximum rate of auroral ionization is at higher altitudes than during active, discrete auroral arc displays. These are the conditions most conducive to successful EXCEDE experiments at Poker Flat and are readily identifiable by photometric meridional scan observations. It should be noted that our conclusions parallel those obtained from the Chatanika Incoherent Scatter Radar insofar as on site observations were compared.

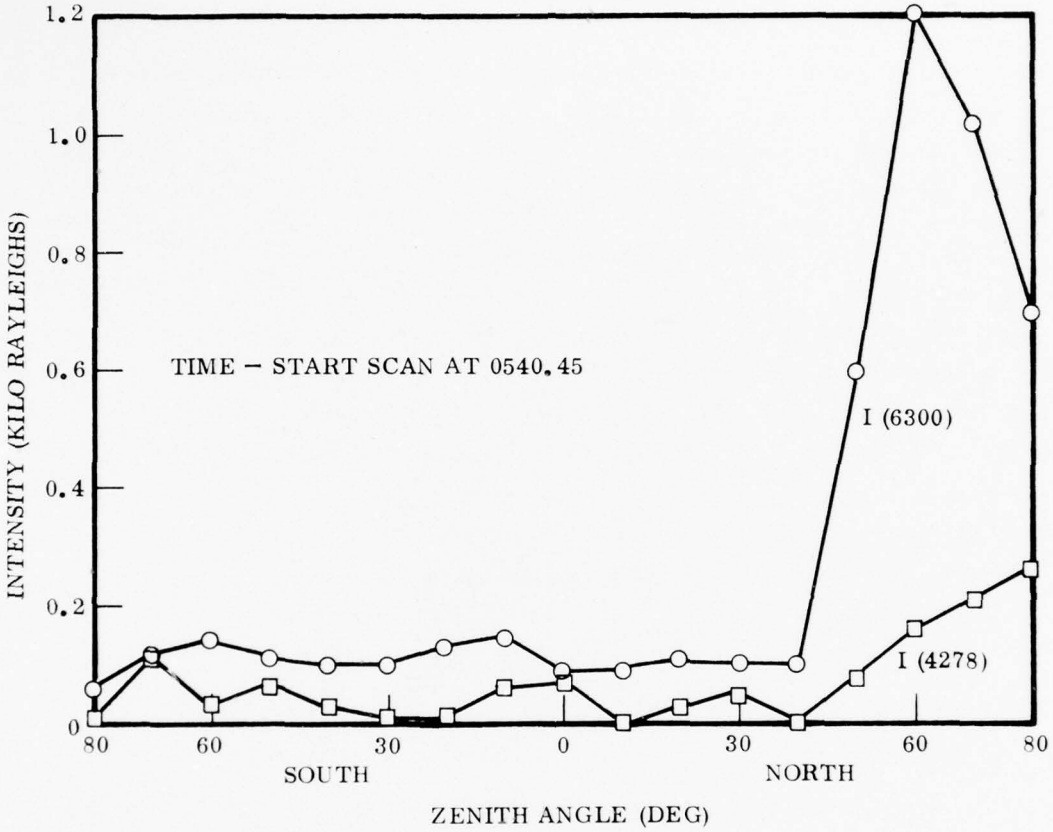

Figure 14 Meridional scan of 4278 Å and 6300 Å intensity for EXCEDE launch of 28 February 1976.

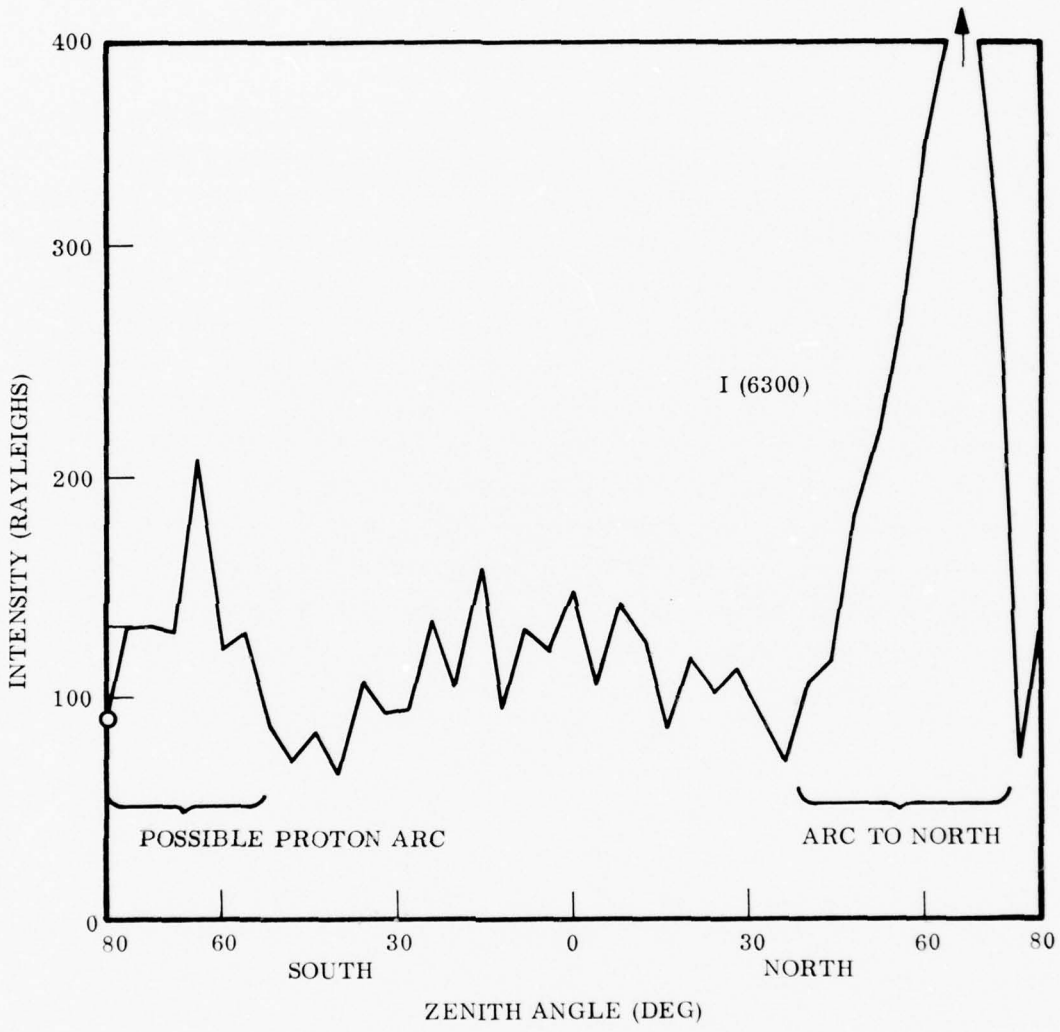

Figure 15 Meridional scan of 6300 Å intensity for EXCEDE launch of 19 November 1976. Intensity enhancement to south is probably caused by a diffuse proton arc. Noise in 4278 Å channel and low intensity level did not allow a meaningful plot.

6. WIDEBAND EXPERIMENT SUPPORT

6.1 Introduction

WIDEBAND experiment support was provided by the meridional scanning three color photometer as well as two three beam photometers observing auroral motions at zenith. The meridional scanning photometer operated on wavelengths 4278A, and 6300A and provided data on total energy deposit in the atmosphere by precipitating particles, total flux of protons (4861A), and intensity of 6300A from OI, which provides the mean energy parameter when ratioed with 4278A as discussed in section 4. The three beam photometers were operated at 5577A and 6300A wavelengths in order to obtain auroral motion data as well as the F-region irregularity motion. The next section discusses the latitudinal distribution of total energy deposit by precipitating electrons and their mean energy parameter. The auroral E-fields are inferred from the 5577A three beam photometer data. Motions of the 6300A, F-region irregularities are presented but a full interpretation of these data is premature insofar as the physical mechanisms creating the observed irregularities and their motions are not fully defined.

6.2 Latitudinal Distribution of Precipitation

The three color photometer was operated in a meridional scan mode such that the latitudinal distribution of the intensities of 4278A, 4861A, and 6300A emissions could be determined during the WIDEBAND rocket launch period. As previously described, the 4278A intensity provides a direct measure of the energy deposit in the field of view by precipitating electrons and protons. The 4861A emission intensity provides a measure of proton particle flux into the atmosphere, and 6300A emission from OI provides a means of obtaining the mean energy parameter of the precipitating electrons as described in chapter 4. In this section, we describe the distribution of energy deposit which is a direct measurement of the ionization source strength, and the concurrent variations of the R_{64} ratio from which the mean energy parameter is derived. We have not reduced and calibrated the 4861A data as yet.

Three consecutive scans of the three beam photometer which were taken immediately after rocket launch at 1025UT are presented in figure 16. Here,

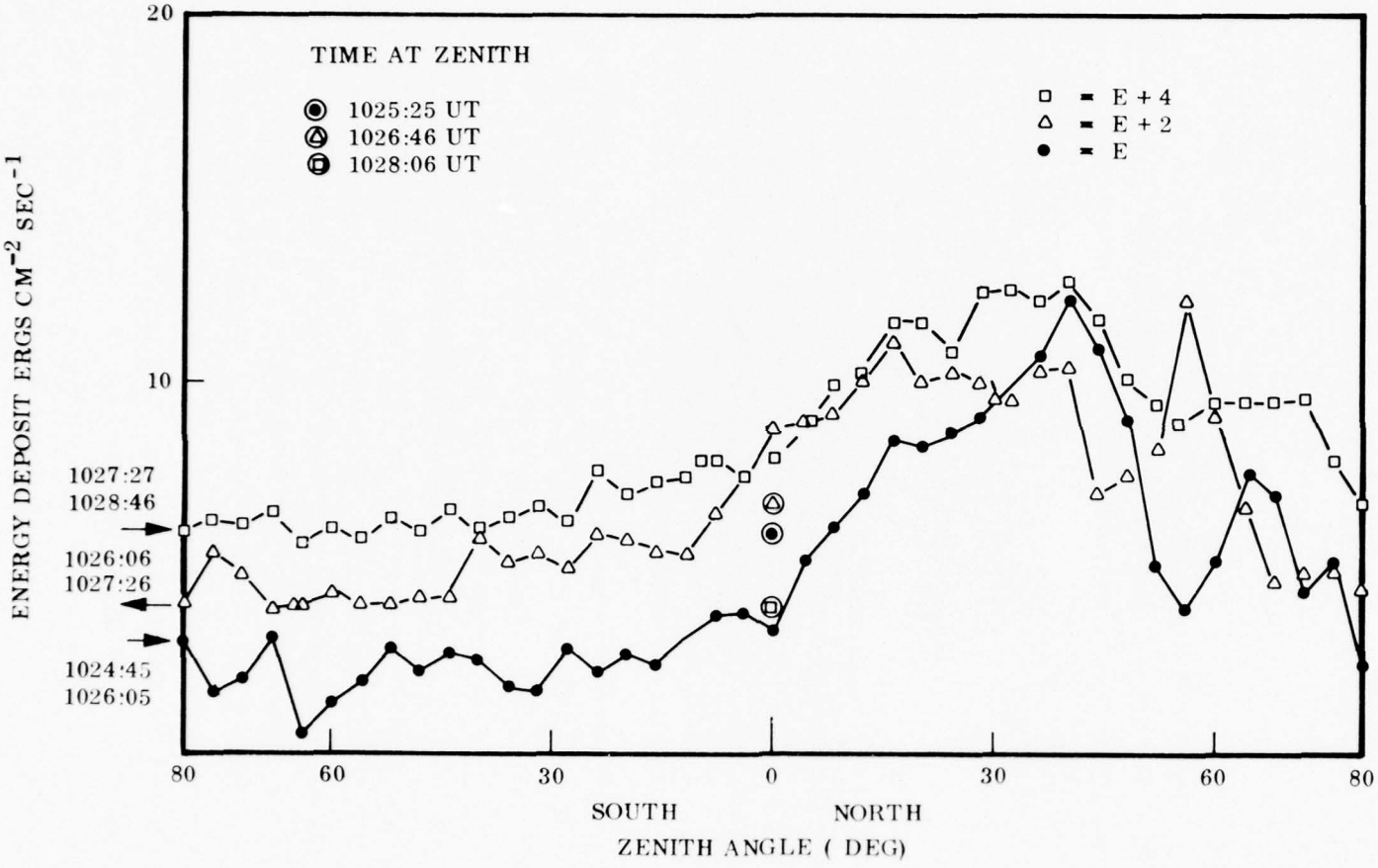

Figure 16 Latitudinal scan of total energy deposit as derived from 4278 Å photometric intensities. Three scans during the flight of WIDEBAND rocket No. 2, 26 November 1976 are presented. Note that the zero level of successive scans indicated by Δ and □ are offset by 2 and 4 ergs/cm^2 sec respectively to separate the curves.

the 4278A intensity vs. zenith angle is converted to the total energy deposited in the atmosphere. The direction and time duration of the scans is indicated on the figure. The zero level for energy deposit also has been shifted by 2 erg cm^{-2} sec^{-1} for consecutive scans in order to separate the curves for clarity. These data show that a weak ionizing flux was present to the south of zenith (approximately 1 to 2 erg cm^{-2} sec^{-1}) gradually increasing in magnitude to zenith. Near zenith, the horizontal gradient in ionizing flux increased indicating that the diffuse precipitation region grows stronger to the north. At greater distances to the north, one or more discrete arcs are observed which is typical for the quiet time diffuse auroral region. It should be noted that in the diffuse precipitation region near zenith the overall intensity changes by nearly a factor of two from scan to scan, but the horizontal gradients appear to remain similar in form. This is clearly not an instrumental effect. Additionally, examination of figure 16 shows that the discrete arc to the north also shifts not only in magnitude but in location as successive scans are made. However, this motion probably does not affect the data obtained on the rocket upleg (at about 10° north zenith angle) because it remains within the diffuse precipitation region.

The mean energy parameter computed from the R_{64} ratio value is presented in figure 17 in a format similar to figure 16. Here, the mean energy increases from a generally soft value in the south to harder, more energetic, values in the north. The discrete arcs show the hardest values of mean energy ranging from about 10 to 15 kev which is consistent with previous observations. An apparent very large mean energy parameter is indicated for some scans in the region of 40 to 60° south zenith angle. These anomalously large values we believe are produced by a geometrical effect which has not been removed from the analysis at this time. The effect is produced by looking out from the edge of the precipitation region wherein the observed 4278A emission is produced by precipitating electrons near 120 km, but the 6300A emission is produced in the F-region (above about 180 kn) outside the region of precipitation. Because the F-region equatorward of the diffuse quiet time auroral zone is depleted of ionization at times much after sunset, the emission of 6300 by electron-ion recombination is greatly reduced consequently producing anomalously low values for the R_{64} ratio. Further improvements in our analytical codes will be

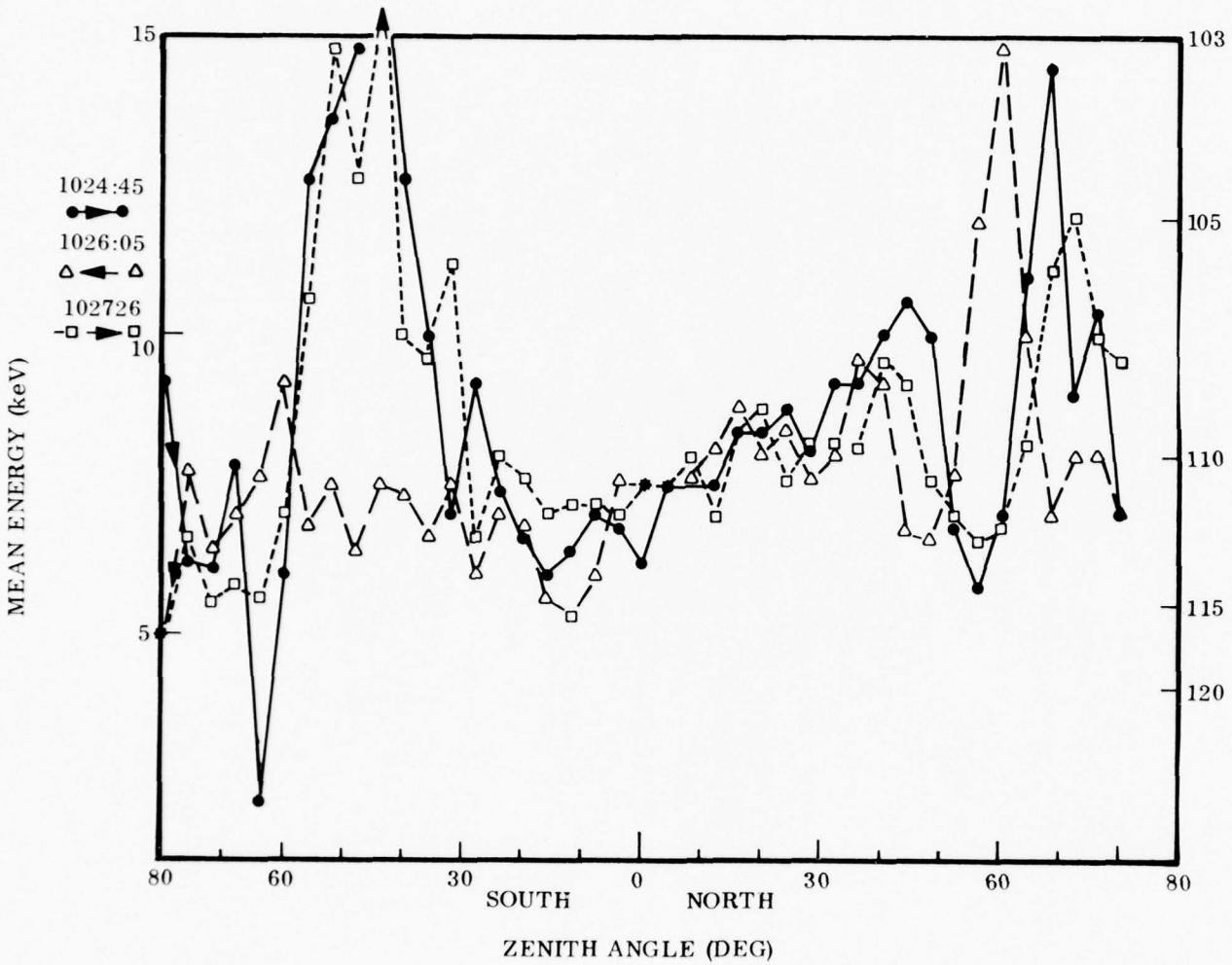

Figure 17 Latitudinal scans of mean energy of precipitating electrons as derived from the photometric intensity ratio R_{64} = I(6300/I(4278 Å). The right hand scale indicates the approximate altitude of peak ionization for the precipitating electrons.

required in order to remove such geometrical artifacts.

The overall behavior of the mean energy parameter vs. zenith angle is closely parallel to the total energy value variations. This suggests that over the diffuse auroral region at least, the total precipitating electron flux is nearly constant vs. latitude but the mean energy increases slowly going from equator to poleward edges. The detailed behavior of the mean energy and energy deposit also shows some small scale features which are apparently real, not statistical artifacts. Similar effects have also been observed in the incoherent scatter radar data. For example, there are optical indications that the small F-region "bubble" observed at zenith angles of approximately 40 degrees to the south is a precipitating particle feature, not a remnant of the daytime F-region. At this time the data have not been fully reduced, consequently we are unable to determine whether this feature might be caused by proton precipitation rather than soft electron precipitation. Further effort to resolve the details of the optical emission features and interpret them in terms useful to the WIDEBAND measurements is required.

6.3 Measurements of Auroral Motions and Irregularities

The three beam photometers were utilized to make auroral motion observations in the 5577A and 6300A emissions. The emission of 5577A in auroras is generated mainly by processes directly related to the auroral electron flux, hence irregularity motions observed in emission accurately depict the flux irregularities and their motion. The 6300A F-region emission however, is more complicated. The oxygen O(1D) state has a radiative lifetime of about 100 seconds, therefore excitation by auroral particles is integrated in time and smeared spatially due to neutral mass motions. An additional complication is the collisional quenching of the 1D state at altitudes below about 180 km, which effectively reduces the observed lifetime of the state. Because of these features, interpretation of the 6300A horizontal phase velocity and other associated quantities is made much more difficult.

Auroral motions observed in the 5577A emission region have been interpreted in terms of the E-fields required to generate the horizontal motions in precipitating particle flux irregularities, i.e., by the ExB forces. Electric

fields deduced by this technique for the period surrounding launch of the WIDEBAND rocket are depicted in figure 18. These E-field values are characteristic of a small region immediated around zenith and may not necessarily be identical to these in the region of the rocket trajectory. However, they probably provide a reasonable representation of the conditions in space which were sampled by the rocket. Additionally, the general behavior of the E-fields inferred photometrically agree qualitatively with the much larger scale fields as sampled by the Chatanika incoherent scatter radar, although the magnitudes appear to differ somewhat. The later term E-field variations, near 1100 UT apparently characterize the extremely large spatial shear in E-fields and auroral plasma motion observed both on satellited, by the Chatanika radar, and by WIDEBAND observations of irregularity motion. It is likely that the shear observed overhead at about 1100 UT is the later time development of shear motion observed at high latitudes during the rocket-satellite experiment at 1025 UT. which were reported by Livingston (private communication).

Observations of E and F-region irregularity motions made with the two three beam photometers are illustrated in figures 19 and 20. Here, the dispersive motion of the 5577A emission fluctuations depicts the auroral motion whereas the 6300A motions is a combination of auroral excitation and drifts of the emitting irregularities. These data are presented for the five minute period following rocket launch and therefore are representative of conditions at zenith averaged over the rocket flight time approximately.

In order to uniquely separate the effects of auroral motion from the neutral and ion motions representative of the observed fluctuations in the F-region, 6300A data, a much more intensive data reduction effort will be required. Qualitative comparisons of the 5577A and 6300A three beam photometer measurements of horizontal phase velocity and other parameters indicates that such an effort should be fruitful. If successful, then the 6300A data will be directly comparable to the WIDEBAND interferometer experiments and will be useful in interpreting these data.

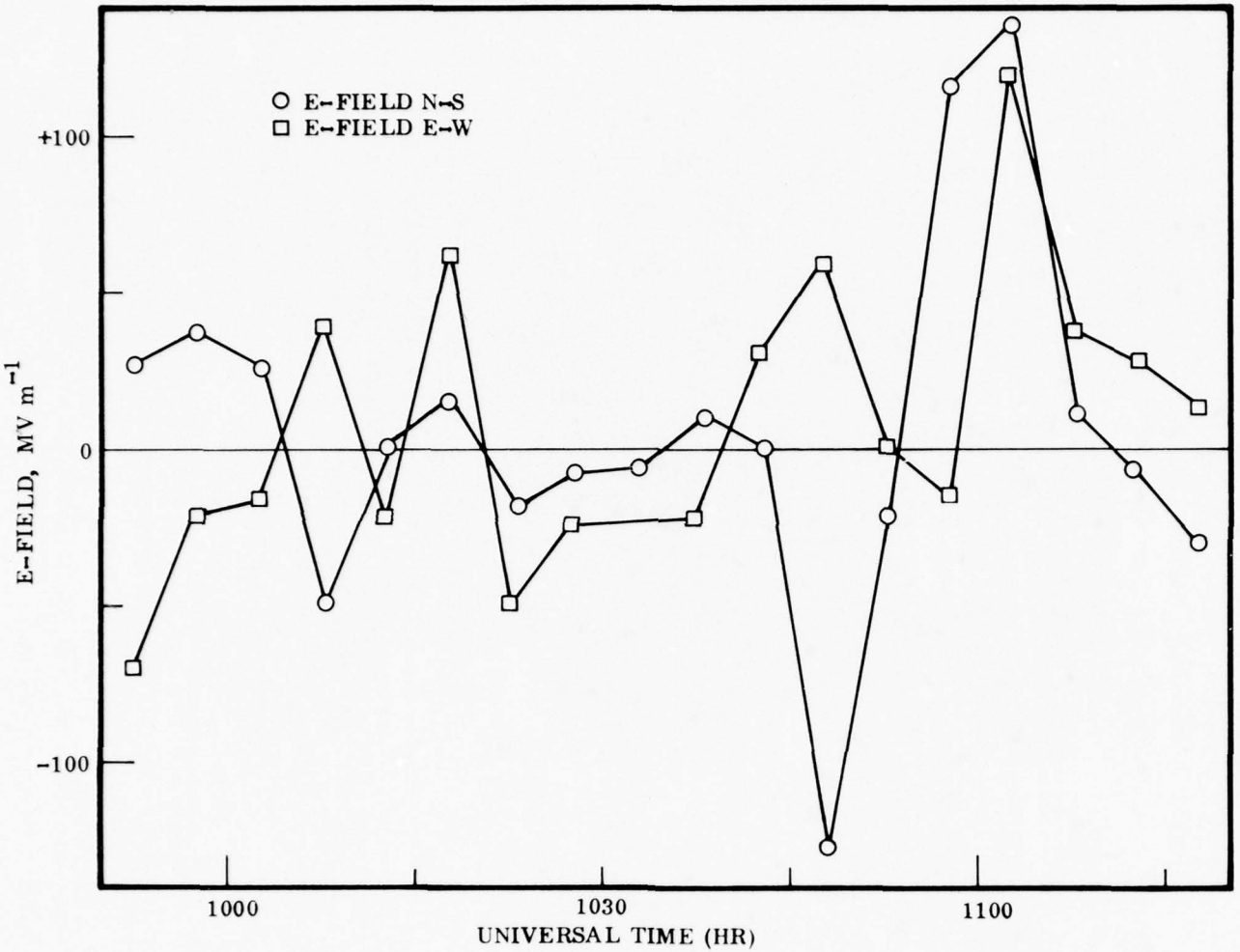

Figure 18 Ionospheric Electric Fields computed from three beam measurements of auroral motions in 5577 Å spectral region for WIDEBAND rocket, 26 November 1976. Launch time 1025 UT.

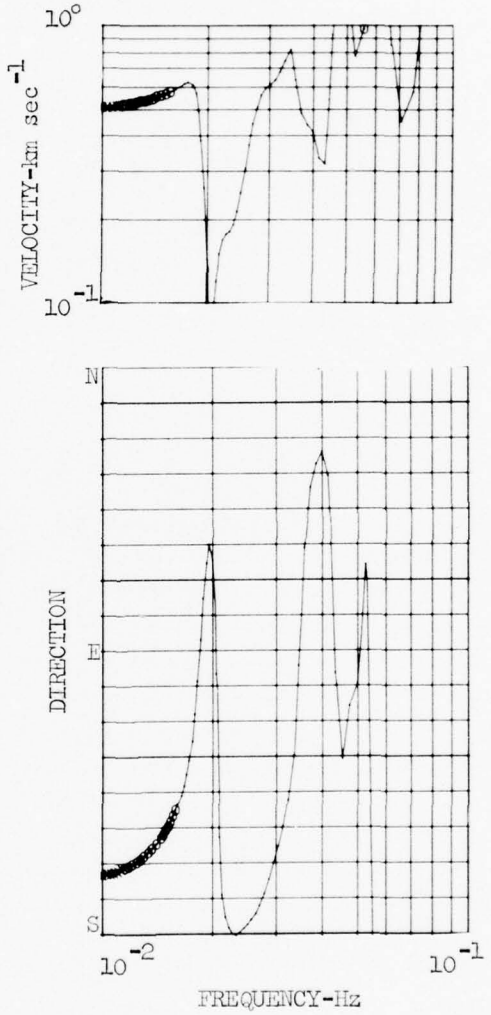

Figure 19 Velocity spectra for auroral motions observed in 5577 Å emission. Upper curve is dispersive velocity, lower curve is direction. Data for WIDEBAND satellite experiment, 26 November 1976.

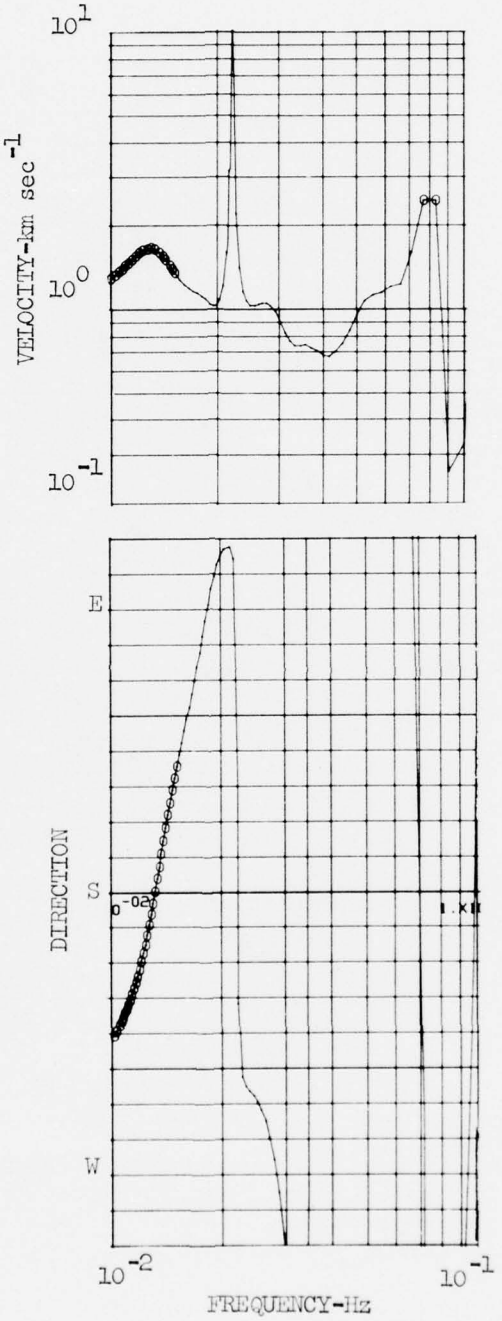

Figure 20 Velocity spectra for auroral motions observed in 6300 Å emission. Data are for WIDEBAND satellite experiment 26 November 1976. Format is similar to Figure 19.

7. SUMMARY AND CONCLUSIONS

7.1 Summary of Experimental Results

The Ionospheric Irregularities Program provided ground based optical supporting measurements to the DNA/HAES Program in Alaska for a number of rocket experiments conducted during the 1976 contract period. Specific rockets which were supported were:

- EXCEDE 28 February 1976
- EXCEDE 19 November 1976
- WIDEBAND 26 November 1976

In addition, ground based support was operated for the ICECAP rocket series which was postponed indefinitely from the February window. These shots were the SWIR/SWIR/TMA series.

The principal results for the EXCEDE rockets were obtained utilizing the meridional scanning three color photometer. The purpose of these measurements was to confirm that a low level of precipitating flux background existed during the EXCEDE flights. Our results indicated that for both flights, although some auroral precipitation activity was present to the north, an acceptably low level of precipitation input was present during the flight at least in the vicinity of its upleg trajectory. The very small degree of precipitation present in the vicinity of the upleg trajectory was diffuse and apparently low in mean energy.

Data obtained in support of WIDEBAND are quite extensive and require much more interpretation than has been conducted to date. We observed a meridional gradient in both total energy deposit and in mean energy parameter during the 26 November coordinated WIDEBAND satellite-rocket experiment. Diffuse visible auroras extended to near zenith from the north indicating that an ionization gradient should exist near zenith. The scanning photometers expanded on this observation and quantified it. Small scale features in both E- and F-region structure observed by the incoherent scatter radar were also observed photometrically and indications of structure in the precipitating flux as well as in the ambient ionosphere were verified. The three beam photometer data on auroral E-fields showed a generally low level, but temporally dynamical E-field behavior.

These data agreed well with the radar. F-region structure and motions as observed in the 6300A OI emission line were very complicated. Dispersive motion was observed wherein the horizontal phase velocity varied significantly in magnitude and direction with frequency. These data also agree qualitatively with the WIDEBAND satellite interferometer receiver data (Livingston et al, private communication) although we have not been able to carry out detailed quantitative comparisons as yet. The WIDEBAND support data require much more effort in reduction and interpretation if they are to be quantitatively useful in analysis of the ionospheric properties which produce the observed scintillation effects on WIDEBAND.

7.2 Summary of Analytical Results

Analytical efforts during the 1976 Ionospheric Irregularities Program were confined to improvement of the three beam data reduction code and to confirming the cross calibration between photometer and incoherent scatter radar measurements of the mean energy parameter of the precipitating electron flux. Code improvements will allow much more flexible use of the three beam photometer technique for measurements of auroral motions, neutral winds and wavelike motions, and their associated quantities.

Perhaps the most important analytical results obtained during 1976 was the cross calibration of photometric and incoherent scatter radar techniques for measurement of the precipitating electron flux mean energy parameter. Theoretical results indicated that for Maxwellian energy distribution in the precipitating electrons, the ratio of emission intensities $R_{64} = I(6300)/I(4278)$ would be a useful measure of the mean energy parameter. Comparisons of the photometric data with equivalent quantities computed via the SRI/UNTANGLE code using incoherent scatter radar data provided a cross calibration between the experimental techniques as well as confirming the theoretical predictions.

This result is important because it will allow use of either photometer or radar measurements of both energy and mean energy parameter in future HAES experiments with more confidence as well as provide additional comparative data for past and/or future nuclear test measurements.

7.3 Ground-based Optics and Future HAES Experiments

Passive ground-based optical support experiments have been limited to detection of the optical emission features from limited altitude regimes characteristic of the emitting species. The Ionospheric Irregularities Program has concentrated upon the well known auroral and airglow emitting species which are listed below:

Species	Wavelength	Altitude of Peak Intensity
OH	near IR and IR	85 km
Na	5896A	95 km
OI	5577A	95 to 120 km
OI	6300A	150 to 300 km
N_2^+	4278A	90 to 150 km

These spectral emission features and their altitude dependences are now reasonably well known, and the features can be interpreted in terms of their causitive phenomenology with confidence. Likewise, application of HAES measurements of the temporal, spatial, and spectral characteristics of these features to further understand the existing high altitude nuclear effects data base is theoretically and analytically supportable. However, we must consider other equally important spectral emission features; for example, emission from O_2 in the atmospheric and infrared atmospheric bands, emission from NO, NO_2 and other infrared active species, and emission from high altitude ionic species such as OII (O^+). Support of future HAES experiments will require such an expansion of the experimental capabilities in order to extend the altitude range accessible to ground- and/or aircraft-based optical support experiments.

In addition to extending the spectral range of optical support experiments, the spatial and temporal dynamical ranges must be extended by means of more flexible instrumentation design. For example, our present three beam photometer experiments are designed to measure auroral and neutral species motions over spatial scales of tens of kilometers. It is now well known that the spatial irregularities which cause scintillation effects, possible infrared irregularities,

and upper atmospheric turbulence scales extend down to the tens of meters sizes or smaller. Thus, it is incumbent that the ionospheric irregularity instrumentation be extended in capability to cover these scale sizes.

Results obtained to date on the Ionospheric Irregularities Program indicate that further valuable support can be provided to the HAES effort in the following areas:

- INFRARED PROGRAMS

  Ground-based infrared measurements of NO fundamental and overtone band radiances utilizing ultranarrowband interference filter radiometry

  Ground-based visible and near IR measurements of excitation of NO precursor species

  Measurements of energy input processes made by combined ground-based optical and incoherent scatter radar experiments

  Measurements of transport processes made by combined optical and radar techniques

- SATELLITE AND RADAR PROPAGATION EFFECTS

  Ground-based optical and scatter radar measurements of plasma properties, especially neutral and ionic motions, plasma gradients, and electron and ion temperatures, both in auroral and equatorial regions

  High resolution optical measurements of auroral precipitation and plasma irregularities

  High resolution optical and radar measurements of equatorial region plasma irregularities, especially those in the F-region

- NUCLEAR BURST PHENOMENOLOGY

  Much interpretative data regarding the burst phenomenology at low latitudes must be obtained if it is to be applied to high latitude battle space conditions. Data regarding neutral and ionospheric wave motions, plasma drifts and irregularities, and other phenomenology conditions must still be obtained in order to fully utilize the existing nuclear test

data base. Optical measurements, especially those related to F-region irregularity generation will be valuable. Most of these are obtainable as supporting efforts for other ad-hoc experiments

In conclusion, it is especially important to point out the value of conducting well coordinated experiments utilizing a variety of observational tools. For example, the continued cooperative experimental and analytical efforts between the Ionospheric Irregularities Program and various programs conducted by SRI utilizing the Chatanika incoherent scatter radar have led to valuable insights into upper atmospheric and auroral phenomenology and its application to the HAES Program. Further efforts of this nature should be strongly encouraged.

REFERENCES

1. Sears, R. D., "Coordinated Measurements of Ionospheric Irregularities: Digital Photometer Design and Development," Topical Report, Contract DASA 01-71-C-0158, LMSC/D311213, Oct. 20, 1972

2. Sears, R. D., "Definition of Energy Input: Operation ICE CAP," Final Report, Contract DNA 01-72-C-0134, DNA 2985F, LMSC/D311131, Oct. 1, 1972

3. Sears, R. D., "Ionospheric Irregularities: Alaska Photometric Measurements," Final Report, Contract DNA 001-73-C-0110, DNA 3235F, Dec. 4, 1973

4. Sears, R. D., Evans, J. E., and Varney, R. N., "ICE CAP Analysis: Mechanisms for Energy Deposit in the Auroral Ionosphere," Interim Final Report on Contract DNA 001-73-C-0224, DNA 3293F, Jan. 15, 1974

5. Sears, R. D., "Ionospheric Irregularities: Auroral Motions and Plasma Drifts," Final Report, Contract DNA 01-74-C-0179, DNA 3514, LMSC/D405729, Sept. 30, 1974

6. Sears, R. D., "ICE CAP Analysis: Energy Deposit and Transport in the Auroral Ionosphere, ICE CAP 73-74," HAES Report No. 5, Final Report DNA 01-73-C-0224, DNA 3566F, Nov. 15, 1974

7. Sears, R. D., "Versatile Family of Modular Aurora and Airglow Photometers," Appl. Optics 12, 1349-1355, 1973

8. Sears, R. D., "Intensity Correlations of the 4278Å N_2^+ (0-1) First Negative Band and 5875Å Emissions in Auroras," J. Geophys. Res. 80, 215-217, 1975

9. Sears, R. D., and Evans, J. E., "Coordinated Optical and Radar Measurements of Auroral Motions and Ionospheric Plasma Drift in Atmospheres of the Earth and Planets," Ed. B. M. McCormac, D. Reidel Pub. Co., 1974

10. Sears, R. D., "Ionospheric Irregularities. HAES Program Support," HAES Report No. 29, Final Report, Contract DNA001-75-C-0098, 30 Sept. 1975

11. Chamberlain, J. W., Physics of the Aurora and Airglow, pp. 128-132, Academic Press, New York, 1961

12. Kamiyama, H., The Dependence of the Relative Intensity of some of the auroral Lines upon the Energy Spectrum of Precipitating electrons, Science Reports of the Tohoku University, 18, 8390, 1967

13. Banks, P. M., Chappel, C. R., and Nagy, A. F., "Spectral Degradation, Backscatter, Optical Emissions, and Ionization," J. Geophys. Res. 79. 1459-1470, 1974

14. Judge, R. J. R., "Electron Excitation and Auroral Emission Parameters," Planet. Space Sci. 20, 2081-2092, 1972

15. Rees, M. H., and Luckey, D., "A New Model for the Interaction of Auroral Electrons with the Atmosphere," J. Geophys. Res. 79, 5181-5186, 1974

16. Wickwar, V. B., Baron, M. J., and Sears, R. D., "Auroral Energy Input from Energetic Electrons and Joule Heating at Chatanika," J. Geophys. Res. 80, 4364, 1975

17. These data are summarized in DNA, Reaction Rate Handbook, ed. M. H. Bortner and T. Baurer, Chapter 9, pp. 9-24 to 9-29, DNA1948H, March 1972. Published by DASIAC

18. Mende, S. B., and Eather, R. H., "Spectroscopic Determination of the Characteristics of Precipitating Auroral Particles," J. Geophys. Res. 80, 3211-3216, 1975

19. Vondrac, R. R., and Baron, M. J., "Radar Measurements of the Latitudinal Variation of Auroral Ionization," Radio Science 11, 939-946, 1976

Appendix A

Chatanika 1976 Data

Synopsis Sheets

SYNOPSIS OF DATA

Tape: WOLFØ1 (60992-FILE 1)

Date:2/10/76 **Time**: 0600 to 1327 OT

Photometer(s): 3B1, 3B2, 3C

General Activity:

Active forms visible from before 0800 to after 1200

Operating Modes:

0647 to 1257-3C-4278, 4861, 6300, zenith
0657 to 1257 3B1 - 5890Å - zenith
0707 to 1257 3B2 - 7700 - zenith

Notes:

3/4 Moon -
OH - NA Program
3B1-E channel very noisey

SYNOPSIS OF DATA

Tape: WOLFØ2 (60992-FILE2)

Date: 2/11/76 **Time:** 0515 to 1330 UT

Photometer(s): 3B1, 3B2, 3C

General Activity:

Active after 0800 to about 1100 UT

Operating Modes:

0550-1300 3B1 on 30 sec dwell, 30 degree incremented SCAN mode (Denote SCAN E) limits zenith 150°N (30° el. angle). 5577Å

0550-1300 3B2 - 5577-zenith

0550-1300 3C - zenith

Notes:

Strong moonlight.

SYNOPSIS OF DATA

Tape: WOLFØ3 (60992-FILE 3)

Date: 2/12/76 **Time:** 0445 to 1250 UT

Photometer(s): 3B1, 3B2, 3C

General Activity:

Low-Auroral arcs detected to north

Operating Modes:

0520 - 1220 - 3B1 - 5577Å - SCAN MODE
0520 - 1220 - 3B2 - 5577Å - zenith
0520 - 1220 - 3C - zenith

Notes:

Strong moonlight

SYNOPSIS OF DATA

Tape: WOLFØ4 (60992 - FILE 4)

Date: 2/13/76 **Time:** 0450 to 1330 UT

Photometer(s): 3B1, 3B2, 3C

General Activity:

Strong near 1200 UT at zenith

Operating Modes:

0520 - 1045 3B1 5588Å, at 155° NL (25° N elevation)
1045 - 1300 3B1, 5577Å, SCAN E Mode
0520 - 1300 3B2, 5577Å, zenith
0520 - 1300 3C, zenith

Notes:

Moon Up
Satellite Passes:
0515 UT AE-C
0932 UT TRIAD

SYNOPSIS OF DATA

Tape: WOLFØ5 (61179-FILE 1)

Date: 2/14/76 **Time**: 0400 to 1335 UT

Photometer(s): 3B1, 3B2, 3C

General Activity:

Low most of evening
0800 Faint arc to north
1100 Intense Ω form extending to zenith
1130 Back to Low activity

Operating Modes:

0440 - 1305 3B1, 5577Å, SCAN E Mode
0440 - 1305 3B2, 5577Å, Zenith
0440 - 1305 3C, zenith

Notes:

Full Moon
Satellite Passes:
0516 AE-C
0741 S3-2
0902 TRIAD
1042 TRIAD
1218 ISIS-1

SYNOPSIS OF DATA

Tape: WOLFØ6 (61179 - FILE 2)

Date: 2/15/76 **Time**: 0600 - 1130 UT

Photometer(s): 3B1, 3B2, 3C

General Activity:

Quiet but very weak arcs to North

Operating Modes:

0645 - 1100 3B1, 5577Å, zenith
0645 - 1100 3B2, 6300Å, zenith
0645 - 1100 3C at zenith

Notes:

Satellite Passes:
0735 UT S3 - 2
1012 UT TRIAD
1149 UT ISIS1

After 1040 Cirrus moving in from south east.
1100 - Cloudy at zenith
1050 to 1130 3CR(ch 10) has abnormally hi CR- to 1010, 3B1 Weak wavelike variations.
0950 - 1000 (46) 3B1 ch 4 has noise, strong wavelike variations 3B1, 3B2

Tape: WOLFØ6 (61179 - FILE 2) Continued----

Notes: continued

0940 - 0945(44) 3B1(4) noise
0935 - 0945(43) 3B1(4) noise
0940 - 0945(42) 3B1(4) noise
0910 - 0945(38) 3B1(2) noise
0740 - 0835(30) 3B1, 3B2, 3C - occasional wavelike variations

SYNOPSIS OF DATA

Tape: WOLF 07 (61179 - FILE 3)

Date: 2/16/76 **Time**: 0500 to 1330 UT

Photometer(s): 3B1, 3B2, 3C

General Activity:

Quiet until 1030 UT

Active to north after 1030 but did not reach zenith.

Operating Modes:

0530 - 0929	3B1, 5890Å on zenith
0930 - 0950	3B2, 7700Å on zenith
0929 - 0930	3B1 and 3B2 on DCR
0950 - 1050	3B1, 5577Å, 155° N angle
	3B2, 5577Å, zenith
1050 - 1315	3B1, 5577Å, 90 to 150° scans
	30° increment 30 sec dwell
	3B2, 5577Å zenith
0530 - 1315	3C on zenith

Notes:

Satellite Passes:

0542 - AE-C
0728 - S3-2
0942 - TRIAD

1120 - 1125 Ut 3CR erratic

Full Moon Period

0930 to 1050	3C noisey (ch 8 and 10)
1015	3C - ch 8 quieted down
1030	Activity in 3B and 3C9 at low level
1050	3C ch 8 noisey, ch 10 off scale

Tape: WOLF 07 (61179 - FILE 3) Continued--

Notes:

Check for possible proton arc after 0930

1115 (76) - 1125(78) 3C very noisey all channels

3B1 activity to north (30° el angle)

1050 - 1200

1145(82) 3C (ch 10) zeroed

1200 - 1225 3B1 activity moved to 120° sector

SYNOPSIS OF DATA

Tape: WOLF08 (61179 - FILE 4)

Date: 2/17/76 Time: 0430-1320 UT

Photometer(s): 3B1, 3B2, 3C

General Activity:

Quiet until 0850
0850 multiple faint arcs to zenith
after 0900 strong activity from north to zenith

Operating Modes:

0500 - 0830	3B1, 5890Å, zenith
	3B2, 7700Å, zenith
0835 - 1250	3B1, 5577Å, SCANS 90° to 150°, 30° angle increment, 30 sec dwell time
	3B2, 5577Å, at zenith
0500 - 1200	3C zenith

Notes:

Moon up after 0620 UT
Satellite passes:

0721 - S3-2
0911 - TRIAD

SYNOPSIS OF DATA

Tape: WOLF09 (57930 - FILE 1)

Date: 2/18/76 Time: 0420 to 1330 UT

Photometer(s): 3B1, 3B2, 3C

General Activity:

0650 Faint glow to zenith, arc tonorth

0830 Very active

1230 Stable arcs to south

Operating Modes:

0500 - 0650	3B1, 5890Å, zenith
0820 - 1300	3B2, 7700Å, zenith
0650 - 0820	3B1, 5577Å, SCAN mode 90° - 150°.
	3B2, 5577Å
0500 - 1300	3C, zenith

Notes:

Satellite pass: TRIAD 1022

Rice Rocket launch: 0706:00

SYNOPSIS OF DATA

Tape: WOLF 10 (57930 - FILE 2)

Date: 2/19/76 **Time**: 0440 to 1320 UT

Photometer(s): 3B1, 3B2, 3C

General Activity:

Active all night

Operating Modes:

0500 - 1250	3B1, 5577Å, SCAN mode 30° to 150°, 30° angle increment, 30 sec dwell time
	3B2, 5577Å, zenith
0510 - 1250	3C, zenith

Notes:

Satellite Pass: TRIAD, 0951 UT

SYNOPSIS OF DATA

Tape: WOLF 11 (57930 - FILE 3)

Date: 2/20/76 **Time**: 0510 to 1325 UT

Photometer(s): 3B1, 3B2, 3C

General Activity:

Active after about 0800 UT

Operating Modes:

0520 - 1310 3B1, 5577, zenith
3B2, 6300, zenith

0525 - 1040 3C, SCAN mode, 10°-170°, angle increment 10°, 5 sec dwell time
3C, Magnetic zenith

Notes:

Satellite Pass: 0921 UT, TRIAD

SYNOPSIS OF DATA

Tape: WOLF 12(57930 - FILE 4)

Date: 2/21/76 **Time**: 0430 to 1310 UT

Photometer(s): 3B1, 3B2, 3C

General Activity:

Very active all night

Operating Modes:

0450 - 1100	3B1, 5577Å, zenith
1120 - 1250	3B2, 6300Å, zenith
1100 - 1120	3B1, 5890Å, zenith 3B2, 7700Å, zenith for Loki Launch
0450 - 1250	3C, SCAN mode

Notes:

Satellite Pass: TRIAD, 0851 UT
0730 Arc coming up
0815 Quiet
0940 Strong Arc to north
1015 - 1030 Strong N-S forms, Ω form to zenith
1030 Wall to wall auroras

SYNOPSIS OF DATA

Tape: WOLF 13 (61066 - FILE 1)

Date: 2/22/76 Time: 0430 to 1220 UT

Photometer(s): 3B1, 3B2, 3C

General Activity:

Some activity to north

Quiet at zenith

Operating Modes:

0500 - 1144	3B1, 5890Å, zenith
0500 - 0917	3B2, 5577Å, zenith
0917 - 1144	3B2, 7700Å, zenith
0510 - 1144	3C, SCAN mode

Notes:

After 1120 UT, 3B2N has noise problem

SYNOPSIS OF DATA

Tape: WOLF 14 (61066 - FILE 2)

Date: 2/25/76 **Time:** 0400 to 1225 UT

Photometer(s): 3B1, 3B2, 3C

General Activity:

Hazy all evening
No auroras visible

Operating Modes:

0430 - 1220	3B1, 5890Å, zenith
0430 - 0630 0750 - 1220	3B2, 7700Å, zenith
0630 - 0750	3B2, 6300Å, zenith
0430 - 1220	3C SCAN mode

Notes:

SYNOPSIS OF DATA

Tape: WOLF 15 (61066 - FILE 3)

Date: 2/26/76 Time: 0450 to 1235 UT

Photometer(s): 3B1, 3B2, 3C

General Activity:

Active most of night after 0800

Operating Modes:

0521 - 1200	3B1, 5890Å, zenith
0521 - 0840	3B2, 7700Å, zenith
0840 - 1200	3B2, 5577Å, zenith
0621 - 1200	3C, SCAN mode

Notes:

Data tape has 1 hr clock error before about 0520 UT

Possible proton arc before very active period

SYNOPSIS OF DATA

Tape: WOLF 16 (61066 - FILE 4)

Date: 2/27/76 Time: 0415 to 1130 UT

Photometer(s): 3B1, 3B2, 3C

General Activity:
Active arcs reach zenith after 0830
Breakup at 0905

Operating Modes:

0500 - 1100	3B1, 5890Å, zenith
0500 - 0830	3B2, 7700Å, zenith
0830 - 1100	3B2, 5577Å, zenith
0515 - 1100	3C, SCAN mode

Notes:

Gain problem on 3B2W at 0900

SYNOPSIS OF DATA

Tape: WOLF 17 (58817 - FILE 1)

Date: 2/28/76 Time: 0430 to 1305 UT

Photometer(s): 3B1, 3B2, 3C

General Activity:

Quiet through Excede launch, active later

Operating Modes:

0500 - 1250	3B1, 5890Å, zenith
	3B2, 5577Å, zenith
	3C, SCAN mode

Notes:

0546:40	Excede launch
1212:50	UTD launch
1010 to 1020,	3B1E has gain problems

SYNOPSIS OF DATA

Tape: WOLF 18 (58817 - FILE 4)

Date: 2/29/76 Time: 0445 to 1235 UT

Photometer(s): 3B1, 3B2, 3C

General Activity:

Very active, auroras at zenith before 0430 UT

Operating Modes:

0500 - 1200	3B1, 5890Å, zenith
	3B2, 5577Å, zenith
	3C, SCAN mode

Notes:

3B1E channel erratic near beginning

3CR channel noisey, ~ 0730 to 0850, required gain changes

SYNOPSIS OF DATA

Tape: WOLF 19 (58817 - FILE 2)

Date: 3/1/76 Time: 0435 to 1200 UT

Photometer(s): 3B1, 3B2, 3C

General Activity:

Quiet until about 0730

Active to zenith later

Sky hazy later

Operating Modes:

0505 - 0515	3B1, 5890Å, zenith
0740 - 1145	3B2, 5577Å, zenith
0515 - 0740	3B1, 5577Å, zenith
	2B2, 6300Å, zenith
0505 - 1145	3C, SCAN mode

Notes:

1045:45 Rice Rocket launch - very active to North

SYNOPSIS OF DATA

Tape: ETU Ø.1 (File 1, Tape # 57651)

Date: 1-14-76 **Time:** 0150 to 0925 OT

Photometer(s): 3B1, 3B2, 3C

General Activity:

Quiet, clear skies until 0800 UT

Hazy after 0830 UT

Operating Modes:

0215 - 0450	3B1, 3934Å	; both at zenith
0450 - 0600	3B1, 5577Å	
0215 - 0900	3B2, 3B2, 6300Å	
0215 - 0900	3C	scan mode (10 to 170°, 4° increment, 2 sec dwell)
		AZ Approx 45° true - To intercept H2O Cloud

Notes:

0318:19	Launch of H2O. Release at + 130 SEC.
0600	3B1 developed HV short

SYNOPSIS OF DATA

Tape: ETU Ø2 (No copy made)

Date: 11-15-76 **Time:** 0330 to 1105

Photometer(s): 3B1, 3B2, 3C

General Activity:

No useful data - cloudy

Operating Modes:

Notes:
Ran system to check 3B1E tube, scan mode, etc.

SYNOPSIS OF DATA

Tape: ETØ3 (FILE 2, TAPE # 57651)

Date: 11-19-76 **Time**: 0315 to 1115 UT

Photometer(s): 3B1, 3B2, 3C

General Activity:

Clear skies

Diffuse aurora to zenith at 0830

Operating Modes:

0325 - 0810 3B1, 5890Å

0820 - 1105 3B1, 5577Å

0325 - 1105 3B2, 6300Å

0325 - 1105 3C, SCAN MODE (10 - 170°, 4°, 2 Sec) MAG. Meridian

Notes:

0406:40 Excede Launch

0810 - 0815 3B1 on DCR and CAL

0415 - 0441 3C on DCR

1029 - 1 3C on DCR and CAL for 1 scan each

1030 - 1045 Reset DCR and CAL on 3C photometer

SYNOPSIS OF DATA

Tape: ETØ4 (FILE 3 TAPE # 57651)

Date: 11-22-76 **Time:** 0335 to 1030 UT

Photometer(s): 3B1, 3B2, 3C

General Activity:

Clear sky - hazy near end
Faint activity to North

Operating Modes:

0414 - 0924	3B1, 5577Å, 3B2, 6300Å
0934 - 1024	3C SCAN MODE (10 - 170°, 4°, 2 Sec)

Notes:

0603 - 0743	3CR problems
0743 -	SCAN HEAD RESET - CHECK SCAN DATA BEFORE THIS TIME

SYNOPSIS OF DATA

Tape: ETU Ø5 (no copy made)

Date: 11/24/76 **Time:** 0215 - 1055 UT

Photometer(s): 3B1, 3B2, 3C

General Activity:

No useful data - cloudy later
Possibly useful twilight run on 3934

Operating Modes:

System operated as check - see ETUØ1

Notes:

SYNOPSIS OF DATA

Tape: ETUØ6 (FILE 4, TAPE # 57651

Date: 11/26/76 **Time:** 0735 to 1130 UT

Photometer(s): 3B1, 3B2, 3C

General Activity:

Skies clear
Activity built up, zenith band at rocket launch time

Operating Modes:

0740 - 1120 3B1, 5577; 3B2, 6300;
3C Scan mode (10 - 170°, 4°, 2 sec).

Notes:

1025:43 Launch of WIDEBAND - HI Rocket

1905 - 0910 all on DCR

0947 - 0952 3C on DCR and CAL, 1 sec each

1058(?) Scan head reset

DISTRIBUTION LIST

DEPARTMENT OF DEFENSE

Director
Defense Advanced Research Proj. Agency
ATTN: LTC W. A. Whitaker
ATTN: Nuclear Monitoring Research
ATTN: Strategic Technology Office

Defense Documentation Center
Cameron Station
12 cy ATTN: TC

Director
Defense Nuclear Agency
2 cy ATTN: RAAE, Charles A. Blank
3 cy ATTN: TITL, Tech. Library
ATTN: TISI, Archives
ATTN: RAEV, Harold C. Fitz, Jr.
ATTN: RAAE, Major John Clark
ATTN: RAAE, Major James W. Mayo

Dir. of Defense Research & Engineering
Department of Defense
ATTN: S&SS (OS)

Commander
Field Command
Defense Nuclear Agency
ATTN: FCPR

Chief
Livermore Division, Field Command, DNA
Lawrence Livermore Laboratory
ATTN: FCPRL

DEPARTMENT OF THE ARMY

Commander/Director
Atmospheric Sciences Laboratory
US Army Electronics Command
ATTN: DRSEL-BL-SY-S, F. E. Niles
ATTN: R. Olsen
ATTN: DRSEL-BL-SY-S, D. Snider
ATTN: H. Ballard

Commander
Harry Diamond Laboratories
2 cy ATTN: DRXDO-NP, F. N. Wimenitz

Commander
US Army Nuclear Agency
ATTN: MONA-WE, J. Berberet

Director
BMD Advanced Tech. Center
Huntsville Office
ATTN: ATC-O, W. Davies
ATTN: ATC-T, Melvin T. Capps

Dep. Chief of Staff for Research, Dev. & Acq.
Department of the Army
ATTN: NCB Division
ATTN: DAMA-CSZ-C
ATTN: DAMA-WSZ-C

DEPARTMENT OF THE ARMY (Continued)

Chief of Engineers
Department of the Army
ATTN: Fernand DePercin

Deputy Chief of Staff for Ops. & Plans
Department of the Army
ATTN: DAMO-DDL, COL D. W. Einsel
ATTN: Dir. of Chem. & Nuc. Ops.

Director
US Army Ballistic Research Labs.
ATTN: Tech. Lib., E. Baicy
ATTN: John Mester
ATTN: J. Heimerl
ATTN: M. Kregl

Commander
US Army Electronics Command
ATTN: DRSEL-PL-ENV, Hans A. Bomke
ATTN: DRSEL
ATTN: Stanley Kronenberg
ATTN: DRSEL-RD-P
ATTN: DRSEL-TL-IR, E. T. Hunter
ATTN: Inst. for Exploratory Research
ATTN: Weapons Effects Section

Commander
US Army Foreign Science & Tech. Center
ATTN: Robert Jones

Commander
US Army Material Dev. & Readiness Command
ATTN: DRXCD-TL
ATTN: DRCCDC, J. A. Bender

Commander
US Army Missile Command
ATTN: DRSMI-ABL
ATTN: Chief, Doc. Section
ATTN: DRSMI-XS, Chief Scientist

Chief
US Army Research Office
ATTN: CRDARD-OCS, Hermann Robl
ATTN: CRDARD-P, Robert Mace

DEPARTMENT OF THE NAVY

Chief of Naval Research
Navy Department
ATTN: Code 461, R. G. Joiner
ATTN: Code 461, Jacob Warner
ATTN: Code 421, B. R. Junker

Commander
Naval Ocean Systems Center
ATTN: Tech. Lib. for T. J. Keary
ATTN: Code 2200, Herbert Hughes
ATTN: Code 2200, Ilan Rothmuller
ATTN: Code 2200, Verne E. Hildebrand
ATTN: Code 2200, Jurgen Richter
ATTN: Code 2200, Richard Pappert
ATTN: Code 2200, William F. Moler

DEPARTMENT OF THE NAVY (Continued)

Director
Naval Research Laboratory
ATTN: Douglas P. McNutt
ATTN: Code 7701, Jack D. Brown
ATTN: Code 2600, Tech. Lib.
ATTN: Code 7127, Charles Y. Johnson
ATTN: Code 7700, Timothy P. Coffey
ATTN: Code 7709, Wahab Ali
ATTN: Code 7750, Darrell F. Strobel
ATTN: Code 7750, Paul Julienne
ATTN: Code 7750, Klaus Hein
ATTN: Code 7750, J. Davis
ATTN: Code 7120, W. Neil Johnson
ATTN: Code 2027, Tech. Lib.
ATTN: Code 7750, Joel Fedder
ATTN: Code 7750, S. L. Ossakow
ATTN: Code 7730, Edgar A. McClean

Officer in Charge
Naval Surface Weapons Center
ATTN: Code WA501, Navy Nuc. Prgms. Off.
ATTN: Code WX21, Tech. Lib.
ATTN: D. J. Land
ATTN: L. Rudlin

Commanding Officer
Naval Intelligence Support Center
ATTN: Document Control
ATTN: Code 40A, E. Blase

Superintendent (Code 1424)
Naval Postgraduate School
ATTN: Code 2124, Tech. Reports Librarian

Commander
Naval Weather Service Command
Naval Weather Service Hqs.
Washington Navy Yard
ATTN: Mr. Martin

DEPARTMENT OF THE AIR FORCE

AF Geophysics Laboratory, AFSC
5 cy ATTN: LKB, Kenneth S. W. Champion
5 cy ATTN: OPR, Alva T. Stair
5 cy ATTN: OPR, J. C. Ulwick
2 cy ATTN: OPR-1, R. Murphy
2 cy ATTN: OPR-1, J. Kennealy

AF Weapons Laboratory, AFSC
5 cy ATTN: SUL
5 cy ATTN: DYT
ATTN: CA
5 cy ATTN: DYM
ATTN: G. J. Fryer
5 cy ATTN: DYC

Commander
ASD
ATTN: ASD-YH-EX, Lt Col Robert Leverette

SAMSO/SZ
ATTN: SZJ, Major Lawrence Doan

AFTAC
5 cy ATTN: TD
2 cy ATTN: Tech. Lib.

DEPARTMENT OF THE AIR FORCE (Continued)

Hq. USAF
ATTN: DLS
ATTN: DLCAW
ATTN: DTL
ATTN: DLXP
ATTN: SDR
ATTN: Tech. Lib.

SAMSO/AW
ATTN: AW

ENERGY RESEARCH & DEVELOPMENT ADMINISTRATION

Division of Military Application
US Energy Research & Dev. Admin.
ATTN: Doc. Con. for Major D. A. Haycock
ATTN: Doc. Con. for Colonel T. Gross
ATTN: Doc. Con. for Donald I. Gale
ATTN: Doc. Con. for David Slade
ATTN: Doc. Con. for F. A. Ross

Los Alamos Scientific Laboratory
ATTN: Doc. Con. for R. A. Jeffries
ATTN: Doc. Con. for C. R. Mehl
ATTN: Doc. Con. for G. Rood
ATTN: Doc. Con. for H. V. Argo
ATTN: Doc. Con. for D. Steinhaus
ATTN: Doc. Con. for J. Judd
ATTN: Doc. Con. for T. Bieniewski
ATTN: Doc. Con. for D. M. Rohrer
ATTN: Doc. Con. for Martin Tierney
ATTN: Doc. Con. for Marge Johnson
ATTN: Doc. Con. for John S. Malik
ATTN: Doc. Con. for William Maier
ATTN: Doc. Con. for S. Rockwood
ATTN: Doc. Con. for Donald Kerr
ATTN: Doc. Con. for W. D. Barfield
ATTN: Doc. Con. for Reference Library
ATTN: Doc. Con. for W. M. Hughes
ATTN: Doc. Con. for E. W. Jones, Jr.
ATTN: Doc. Con. for John Zinn
ATTN: Doc. Con. for E. A. Bryant

University of California
Lawrence Livermore Laboratory
ATTN: G. R. Haugen
ATTN: A. Kaufman
ATTN: D. J. Wuebbles
ATTN: J. F. Tinney
ATTN: Julius Chang
ATTN: Tech. Info. Dept.
ATTN: W. H. Duewer

Sandia Laboratories
ATTN: Doc. Con. for W. D. Brown
ATTN: Doc. Con. for Org. 9220
ATTN: Doc. Con. for Craig Hudson
ATTN: Doc. Con. for J. C. Eckardt
ATTN: Doc. Con. for C. W. Gwyn
ATTN: Doc. Con. for D. A. Dahlgren
ATTN: Doc. Con. for M. L. Kramm
ATTN: Doc. Con. for T. Wright
ATTN: Doc. Con. for Charles William
ATTN: Doc. Con. for Sandia Rpt. Coll.
ATTN: Doc. Con. for Doc. Con. Div.

Sandia Laboratories
Livermore Laboratory
ATTN: Doc. Con. for Thomas Cook

ENERGY RESEARCH & DEVELOPMENT ADMINISTRATION
(Continued)

Argonne National Laboratory
Records Control
ATTN: Doc. Con. for A. C. Wahl
ATTN: Doc. Con. for S. Gabelnick
ATTN: Doc. Con. for J. Berkowitz
ATTN: Doc. Con. for Lib. Services Rpts. Sec.
ATTN: Doc. Con. for Len Liebowitz
ATTN: Doc. Con. for David W. Green
ATTN: Doc. Con. for Gerald T. Reedy

US Energy Research & Dev. Admin.
Div. of Hqs. Services
Library Branch G-043
ATTN: Doc. Con. for D. Kohlstad
ATTN: Doc. Con. for J. D. LaFleur
ATTN: Doc. Con. for Class Tech. Lib.
ATTN: Doc. Con. for George Regosa
ATTN: Doc. Con. for Rpts. Section
ATTN: Doc. Con. for R. Kandel
ATTN: Doc. Con. for H. H. Kurzwek

OTHER GOVERNMENT AGENCIES

Department of Commerce
Office of Telecommunications
Institute for Telecom Science
ATTN: William F. Utlaut

DEPARTMENT OF DEFENSE CONTRACTORS

Aero-Chem. Research Laboratories, Inc.
3 cy ATTN: A. Fontijn

AeroDyne Research, Inc.
ATTN: F. Bien
ATTN: M. Camac

Aerospace Corporation
ATTN: Harris Mayer
ATTN: Thomas D. Taylor
ATTN: R. Grove
ATTN: R. D. Rawcliffe
ATTN: R. J. McNeal

University of Denver
Colorado Seminary
Denver Research Institute
ATTN: Sec. Officer for Mr. Van Zyl
ATTN: Sec. Officer for David Murcray

General Electric Company
TEMPO-Center for Advanced Studies
5 cy ATTN: DASIAC, Art Feryok
ATTN: Warren S. Knapp

General Research Corporation
ATTN: John Ise, Jr.

Geophysical Institute
University of Alaska
3 cy ATTN: Neal Brown
ATTN: T. N. Davis

Honeywell Incorporated
Radiation Center
ATTN: W. Williamson

DEPARTMENT OF DEFENSE CONTRACTORS (Continued)

Institute for Defense Analyses
ATTN: Hans Wolfhard
ATTN: Ernest Bauer

Lockheed Missiles & Space Company, Inc.
ATTN: John Kumer
ATTN: John B. Cladis, Dept. 52-12
ATTN: Billy M. McCormac, Dept. 52-54
ATTN: Tom James
ATTN: J. B. Reagan, D/52-12
ATTN: Martin Walt, Dept. 52-10
ATTN: Richard G. Johnson, Dept. 52-12
ATTN: Robert D. Sears, Dept. 52-14

Mission Research Corporation
ATTN: D. Archer
ATTN: P. Fischer

Photometrics, Inc.
ATTN: Irving L. Kofsky

Physical Dynamics, Inc.
ATTN: Joseph B. Workman

Physical Sciences, Inc.
ATTN: Kurt Wray

R & D Associates
ATTN: Robert E. LeLevier
ATTN: Forrest Gilmore

R & D Associates
ATTN: Herbert J. Mitchell

The Rand Corporation
ATTN: James Oakley

Science Applications, Inc.
ATTN: Daniel A. Hamlin

Space Data Corporation
ATTN: Edward F. Allen

Stanford Research Institute
ATTN: M. Baron
ATTN: Ray L. Leadabrand
ATTN: Walter G. Chestnut

Stanford Research Institute
ATTN: Warren W. Berning

Technology International Corporation
ATTN: W. P. Boquist

Utah State University
ATTN: Doran Baker
ATTN: Kay Baker
ATTN: C. Wyatt
ATTN: D. Burt

VisiDyne, Inc.
ATTN: Henry J. Smith
ATTN: L. Katz
ATTN: J. W. Carpenter
ATTN: William Reidy
ATTN: T. C. Degges
ATTN: Charles Humphrey